REFERENCES

Bhat, N.V., Gadre, A.P., and Bambole, V.A. (2003) Investigation of Electropolymerized Polypyrrole Composite Film: Characterization and Application to Gas Sensors. Journal of Applied Polymer Science, 88, 22-29.

Blackwood, D. and Josowicz, M. (1991) Work function and spectroscopic studies of interaction between conducting polymers and organic vapors. The Journal of Physical Chemistry, 95, 493-502.

Brady, S., Lau, K.T., Megill, W., Wallace, G.G., and Diamond, D. (2005) The development and Characterisation of conducting polymeric-based sensing devices. Synthetic Metals, 154, 25-28.

Chandrasekhar, P. (2002) Conducting Polymers, Fundamentals and Applications : A practical Approach. Boston : Kluwer Academic Plublishers.

Chuapradit, C., Wannatong, R. L., Chotpattananont, D., Hiamtup, P., Sirivat, A., and Schwank, J. (2005) Polyaniline/zeolite LTA composites and electrical conductivity response towards CO. Polymer, 46, 947–953.

Collins, G.E., and Buckley, L.J. (1996) Conductive polymer coated fabrics for chemical sensing. Synthetic Metals, 78, 93-101.

Dale, J. (1957) Acta Chemica Scandinavia, 11, 640.

Densakulprasert, N., Wannatong, L., Chotpattananont, D., Hiamtup, P., Sirivat, A., and Schwank, J. (2005) Electrical conductivity of polyaniline/zeolite composites and synergetic interaction with CO. Materials Science and Engineering B, 117, 276-282.

Dyer, A. (1988) An Introduction to Zeolite Molecular Sieves. Chichester : John Wiley & Son. Ltd.,

Enzel, P., and Bein, T. (1989) Inclusion of Polyaniline Filaments in Zeolite Molecular Sieves. The Journal of Physical Chemistry, 93, 6270-6272.

Froyer, G., Maurice, F., Goblot, J.Y., Fauvarque, J.F., Petit, M.A., and Digua, A. (1985) IR Behaviour, conductivity and stability of $FeCl_3$-doped polyparaphenylene $(p\text{-}C_6H_4)_x$. Molecular Crystals and Liquid Crystals, 118, 305-308.

Fukui, K., and Nishida, S. (1997) CO gas sensor based on Au-La_2O_3 added SnO_2 ceramics with siliceous zeolite coat. Sensors and Actuators B, 45, 101-106.

Gangopadhyay, R., and De, A. (2001) Conducting polymer composites : novel materials for gas sensing. Sensors and Actuators B, 77, 326-329.

George, A., Bang, R.L., Lari A.R., Gang, R. K., and Kanjoor, J.R., (2000) Liquid ammonia injury. Burns, 26, 409-413.

Grennan, K., Killard, A.J., Hanson, C.J., Cafolla, A.A., Smyth, M.R. (2006) Optimisation and characterisation of biosensors based on polyaniline, 68, 1591–1600.

Hong, K.H., Oh, K.W., and Kang, T.J. (2004) Polyaniline-Nylon 6 Composite Fabric for Ammonia Gas Sensor. Journal of Applied Polymer Science, 92, 37-42.

Huang, H., Zhou, J., Chen, S., Zeng, J., and Huang, Y. (2004) A highly sensitive QCM sensor coated with Ag^+ ZSM-5 film for medical diagnosis. Sensors and Actuators B, 101, 316-321.

Hugon, O., Sauvan, M., Benech, P., Pijolat, C., and Lefebvre, F. (2000) Gas separation with a zeolite filter, application to the selectivity enhancement of chemical sensors. Sensors and actuators B, 67, 235-243.

Ivory, M.D., Miller, G.G., Sowa, J.M. Shacklette, L.W., Chance, R.R., and Baughman, R.H. (1979) Highly conducting cgarge-transfer complexs of poly(*p*-phenylene). Journal of Chemical Physics, 71(3), 1506-1507.

Jain, S., Chakane, S., Sumui, A.B., Krishnamurthy, V.N., and Bhoraskar, S.V. (2003) Humidity sensing with weak acid-doped polyaniline and its composites. Sensors and Actuators B, 96, 124-129.

Jang, J., and Bae, J. (2006) Carbon nanofiber/polypyrrole nanocable as toxic gas sensor. Sensors and Actuators B, To be plublished.

Kaden, H., Jahn, H., and Berthold, M. (2004) Study of the glass/polypyrrole interface in an all-solid-state pH sensor. Solid State Ionics, 169, 129–133.

Kovacic, P., and Kyriakis, A. (1963) Polymerization of Benzene to *p*-Polyphenyl by Aluminum Chloride-Cupric Chloride. Journal of the American Chemical Society, 85, 454-458.

Kovacic, P., and Oziomek, J. (1964) *p*-Polyphenyl from Benzene-Lewis Acid Catalyst-Oxidant Reaction Scope and Investigation of Benzene-Aluminum Chloride-Cupric Chloride System. Journal of Organic Chemistry, 29, 100-104.

Kumar, D., and Sharma, R.C. (1998) Advance in conductive polymers. European Polymer Journal. 34, 1053-1060.

Kuroda, Y., and Yoshikawa, Y. (1999) Characterization of specific N_2-adsorption site existing on CuZSM-5 type zeolite: effect of ion-exchange level on adsorption properties. The Journal of Physical Chemistry B, 103, 2155-2164.

Kvarnstrom, C., and Ivaska, A. (1997) Characterization and Applicaion of Poly(*p*-Phenylene) and Poly(*p*-Phenylenevinylene), p. 487 in Nalwa, H.S. (Ed.). Handbook of Organic Conductive Molecules and Polymers. Vol. 4. New York : John Wiley & Son Ltd.

Kvarnstrom, C., and Ivaska, A. (1994) Spectroelectrochemical study of polyphenylene by in situ external reflection FT-IR spectroscopy II cyclic voltametry of polyphenylene. Synthetic Metals, 62, 133-139.

Lacaze, P.C., Aeiyach, S., and Lacroix, J.C. (1997) Poly(*p*-Phenylene): Preparation Techniques and properties, p. 205 in Nalwa, H.S. (Ed.). Handbook of Organic Conductive Molecules and Polymers. Vol. 2. New York : John Wiley & Son Ltd.

Li, G., and Kawi, S. (1999) MCM-41 modified SnO_2 gas sensors: sensitivity and selectivity properties. Sensors and Actuators B, 59, 1-8.

Lin, C.W., Hwang, B.J., and Lee, C.R. (1998) Methanol sensors based on the conductive polymer composites from polypyrrole and poly(vinyl alcohol). Materials Chemistry and Physics, 55, 139-144.

Mark, E.D., and Raul, F.L. (1992) Zeolite and Molecular Sieve Synthesis. Chemistry of Materials, 4(4), 756-768.

Marvel, C.S., and Hartzell, G.E. (1959) Preparation and aromatization of poly-1,3-cyclohexane. Journal of the America Chemical Society, 81, 448-452.

Migdilski, J., Blaz , T., and Lewenstam , A. (1996). Conducting polymer-based ion-selective electrodes. Analytica Chimica Acta, 322, 141- 149.)

Niu, X., Zhong, H., Wang, X., and Jiang, Kai. (2006) Sensing properties of rare earth oxide doped In_2O_3 by a sol–gel method. Sensors and Actuators B: Chemical, 115(1), 434-438.

Nohria, R., Khillan, R.K., Su Y., Dikshit, R., Lvov, Y., and Varahramyan, K. (2006) Humidity sensor based on ultrathin polyaniline film deposited using layer-by-layer nano-assembly. Sensors and Actuators, 114, 218–222.

Persaud, K.C. (2005) Polymer in chemical sensing. Materials Today, 8, 38-44.

Pham, M.C., Aeiyach, S., Moslih, J., Soubiran and Lacaze, P.C. (1990) An in situ multiple internal reflection fourier transform infrared spectroscopic (MIRFTIRS) investigation of the growth mechanism of polyphenylene during electrooxidation of biphenyl in methylene dichloride. Journal of Electroanalytical. Chemistry. 277, 327-336.

Prissnaroon, W., Ruangchauy, L., Sirivat, A., and Schwank, J. (2000). Electrical conductivity reponss of dodecylbenzene sulfonic acid-doped polypyrrole film to SO2-N2 mixtures. Synthetic Metals, 114, 65-72.

Rakovic, D., Kostic, R., Gribov, L.A., Stepanyan, S.A., and Davidova, I.E. (1991) Vibration spectroscopy and comparative study of trans-polyacetylene, poly(*p*-phenylene) and poly(*p*-phenylenevinylene). Synthetic Metals, 41, 275-278.

Rauch, W.L., and Liu, M. (2003) Development of a selective gas sensor utilizing a perm-selective zeolite membrane. Journal of Materials Science, 38, 4307-4317.

Reemts, J., Parisi, J., and Schlettwein, D. (2004) Electrochemical growth of gas-sensitive polyaniline thin films across an insulating gap. Thin Solid Films, 466, 320-325.

Rosa, R.M., Szulc, R.L., Li, R.W.C., and Gruber, J. (2005) Conducting Polymer-Based Chemiresistive Sensor for Organic Vapours. Die Makromolekulard Chemie : Macromolecular Symposia, 229, 138-142.

Sahner, K., Schonauer, D., Moos, R., Matam, M., and Post, M.L. (2006) Effect of electrodes and zeolite cover layer on hydrocarbon sensing with *p*-type perovskite $SrTi_{0.8}Fe_{0.2}O_{3-\delta}$ thick and thin films. Journal of Materials Science, 41, 5828–5835.

Schaf, O., Ghobarkar, H., and Guth, U. (1997) Sensors for combustible gas components using modified single crystal zeolites. Ionics, 3, 282-288.

Schaf, O., Wernert, V., Ghobarkar, H., and Knauth, P. (2006) Microporous stilbite single crystals for alcohol sensing. Journal of Electroceramics, 16, 93–98.

Shacklette, L.W., Eckhardt, H., Chance, R.R., Miller, G.G., Ivory, D.M., and Baughman, R.H. (1980) Solid-state synthesis of highly conducting polyparaphenylene from crystalline oligimers. The Journal of Chemical Physics, 73, 4098-4102.

Shiga, T., Okada, A., and Kurauchi, T. (1993) Electroviscoelastic effect of polymer blends consisting of silicone elastomer and semiconducting polymer particles. Macromolecules, 26, 6958-6963.

Soontornworajit, B., Wannatong, L., Hiamtup, P., Niamlang, S., Chotpattananont, D., Sirivat, A., and Schawank, J. (2007) Induced interaction between polypyrrole and SO_2 via molecular sieve 13X. Material Science and Engineering B, 136, 78-86.

Soubiran, P., Aeiyach, S., Aaron, J.J., Delamar, M., and Lacaze, P.C. (1988a) Electrosynthesis and spectroscopic characterization of poly-*para*-phenylene films prepared by oxidation of benzene in liquid sulfur dioxide. Journal of Electroanalytical Chemistry. 251, 89-102. Aeiyach, S., Soubiran, P.; and Lacaze, P.C. (1998b) Influence of the temperature on the structure of poly(*p*-phenylene) (PPP) films formed by electropolymerization of benzene on platinum electrodes in sulphur dioxide medium. Polymer Communications, 29, 130-131.

Srivastava, A., Jain, K., Rashmi, Srivastava, A.K., and Lakshmikumar, S.T. (2006) Study of structural and microstructural properties of SnO_2 powder for LPG and CNG gas sensors. Materials Chemistry and Physics, 97(1), 85-90.

Stankova, M., Vilanova, X., Llobet, E., Calderer, J., Vinaixa, M., Gràcia, I., Cané, C., and Correig, X. (2006) On-line monitoring of CO_2 quality using doped WO_3 thin film sensors. Thin Solid Films, 500(1-2), 302-308.

Su, B-L., Norberg, V., and Hansenne, C. (2000) Infraread spectroscopic study on the location of benzene in KL zeolite upon coadsorption of ammonia and methylamine. Langmuir, 16, 1132-1400.

Venkatathri N., (2006) Influence of aluminium content on synthesis and characterization of different zeolites obtained from ethylene diamine template. Bulletin of the Catalysis Society of India, 5, 17-25

Vilaseca, M., Yague, C., Coronas, J., and Santamaria, J. (2006) Development of QCM sensors modified by $AlPO_4$-18 films. Sensors and Actuators B, 117, 143-150.

Vilaseca, M., Coronas, J., Cirera, A., Cornet, A., Morante, J.R., and Santamaria, J. (2003) Use of zeolite films to improve sensitivity of reactive gas sensors. Catalysis Today, 82, 179-185.

Wagh, M.S., Jain, G.H., Patil, D.R., Patil, S.A., and Patil, L.A., (2006). Modified zinc oxide thick film resistors as NH_3 gas sensor. Sensors and Actuators B, 115(1), 128-133.

Watcharaphalakorn, S., Ruangchuay, L., Chotpattananont, D., Srivat, A., and Schwank, J. (2005) Polyaniline/polyimide blends as gas sensors and electrical conductivity response to CO–N_2 mixtures. Polymer International, 54, 1126–1133.

Wu, C.G., and Bein, T. (1994) Conducting polyaniline filaments in mesoporous channel host. Science, 264, 1757-1759.

Yamamoto, K., and Gu, H.B. (1986) Effect of Ammonium Gas on Electrical Property of Conductive Polymers. Japanese Journal of Applied Physics, 25(7), 1064-1068.

Yaniger, S.I., Rose, D.J., McKenna, W.P., and Eyring, E.M. (1984) Photoacoustic infrared spectroscopy of doped and undoped poly(*p*-phenylene). Macromolecules, 17, 2579-2583.

Yin, F., Blumenfeld, L., Gruver, V., and Fripait, J.J. (1997) NH_3 as a probe molecule for NMR and IR study of zeolite catalyst acidity. The Journal of Physical Chemistry, 101, 1824-1830.

Yli-Lahti, P., Stubb, H., Isotalo, H., Kuivalainen, P., and Kalervo, L. (1985) IR behaviour, conductivity and stability of FeCl3-doped polyparaphenylene (*p*-$C_6H_4)_x$. Molecular Crystals and Liquid Crystals, 118, 305-308.

Zhu, W., Tan, O.K., Yan, Q., and Oh, J.T. (2000) Microstructure and hydrogen gas sensitivity of amorphous $(Ba,Sr)TiO_3$ thin film sensors. Sensors and Actuators B, 65(1-3), 366-370.

Zhou, J., Li, P., Zhang, S., Long, Y., Zhou, F., Huang, Y., Yang, P., and Bao, M., (2003) Zeolite-modified microcantilever gas sensor for indoor quality control. Sensors and Actuators B, 94, 337-342.

APPENDICES

Appendix A Investigation of Characteristic Peaks of FT-IR Spectrum of Undoped and Doped Poly(*p*-phenylene)

FT-IR spectrometer (Nicolet/Nexus 670) was used to characterize functional groups of undoped and doped poly(*p*-phenylene) at 50:1 mole ratio of dopant to moomer unit (uPPP and 50:1 dPPP) and operated in the absorption mode in a wavenumber range of 4000-400 cm^{-1} with 32 scans and ±4 cm^{-1} resolution. Optical grade potassium bromide (KBr) was used as a background material and dried before being mixed with PPP at a ratio of 20:1.

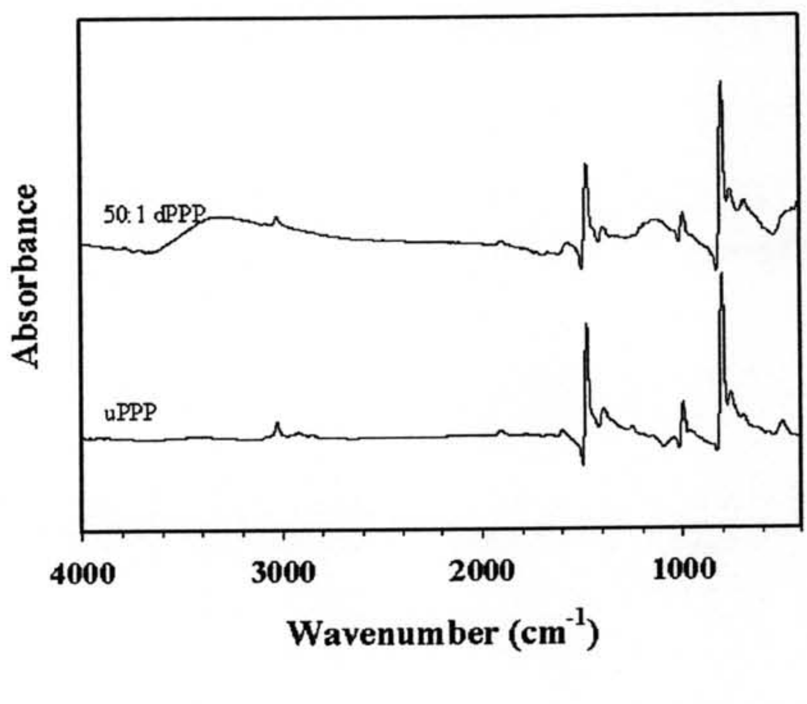

Figure A1 The FT-IR spectra of uPPP and 50:1 dPPP.

The FT-IR spectrum of PPP synthesized by Kovacic's direct route (Kovacic *et al.*, 1963) through oxidative cationic polymerization was shown in Figure A-1. The characteristic absorption peak situated at 805 cm^{-1} was corresponding to *para* aromatic substitution. The less intense absorption peaks occurred at 763 and 695 cm^{-1} were assignable to mono substitution of benzene rings. Moreover, there were additional bands of secondary intensity of *para* band located at 999, 1396, and 1479 cm^{-1} (Kovacic *et al.*, 1963). The several precise assignments of characteristic FT-IR spectrum for PPP were summarized in Table A-1 (Kvarnstrom *et al.*, 1997; Lacaze *et al.* 1997).

The doping of PPP caused the occurrence of new absorption peaks at 1545 and 1180 cm^{-1}that were not appeared in the undoped state of PPP. The doping induced IR characteristic peaks were not due to specific vibrations of dopant molecules or between the molecules and the polymer chain, because the similar peaks appeared for K-, AsF_5- and $FeCl_3$-doping, therefore they are intrinsic vibration of the polymer chain in doping state (Yli-Lahti *et al.*, 1985; Shacklette *et al.*, 1980; Yaniger *et al.*, 1984).

Table A1 Typical IR assignments of uPPP

Wavenumber (cm^{-1})	**Characteristic bands**	**References**
3026±0.6 [3029]	C-H stretching of aromatic	Dale, 1957 and Castiglioni *et al.*, 1989
1599±0.6 [1600]	Quinoid structure	Pham et al., 1990
1396±2.0, 1479±0.4 [1390, 1480]	C-C stretching of aromatic	Pham *et al.*, 1990
999±0.5, 1250±4.0 [1000, 1255]	C-H in-plane vibration of para disubstituted phenyl rings	Soubiran *et al.*, 1998
805±0.6 [817-805]	C-H out of plane vibration of para disubstituted phenyl rings	Froyer *et al.*, 1985
763±2.0 [760]	C-H out of plane vibration mono substituted phenyl rings	Kvarnstrom *et al.* 1985
695±1.0 [692]	C-H out of plane vibration of mono substituted phenyl rings	Rakovic *et al.*, 1991

Appendix B Thermal Property of uPPP and 50:1 dPPP

The thermal property of uPPP and 50:1 dPPP was examined by a thermal gravimetric technique. Thermal Gravimetric Analyzer (duPont/TGA 2950) was used in operating mode: heating rate of 10 °C/min and temperature scan from 30-800 °C under air atmosphere. There was single transition step of both uPPP and dPPP decomposition under air atmosphere. Single transition of uPPP and dPPP decomposition under air atmosphere was noticed as shown in Figure B-1. It was obviously observed that uPPP is thermally and thermooxidatively stable. There was no significant decomposition appeared below 400 °C. It meant that at temperature up to 400 °C uPPP demonstrated good resistance to thermal degradation and air oxidation (Kovacic *et al.*, 1963). At approximately 569 °C PPP backbone began to decompose responsible for the loss of benzene.

dPPP proposed less thermal stability with gradually decomposed when temperature increased, than the undoped one, because doping induced the defect in the polymer chain. However, dPPP still withstand the heat until most of dPPP molecule decomposed at around 480 °C. Moreover, after decomposition dPPP had higher amount of residue than uPPP due to the addition of ferric chloride dopant.

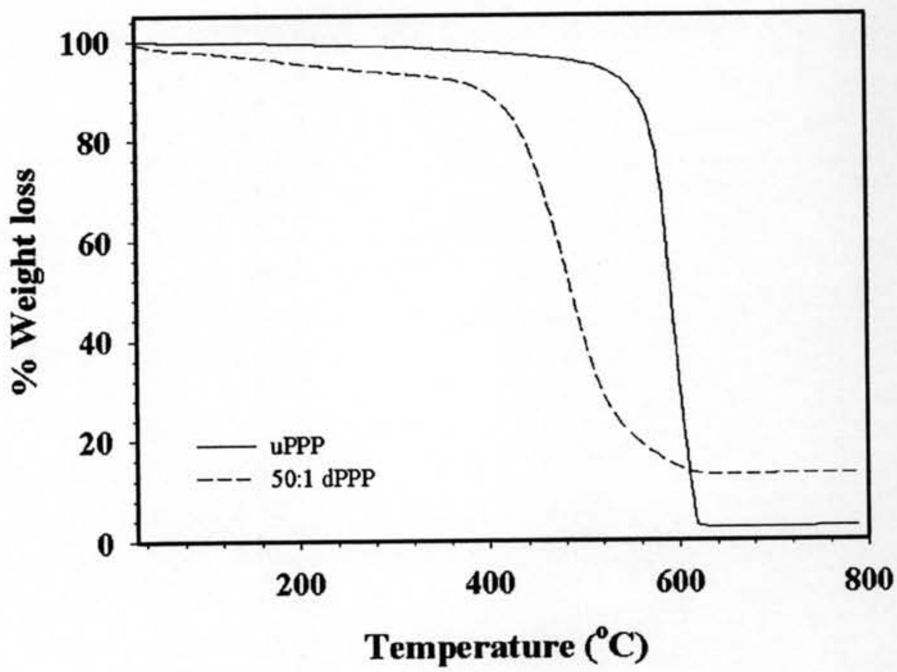

Figure B1 TGA thermogram of uPPP and 50:1 dPPP.

Table B1 Decomposition of uPPP and 50:1 dPPP

Sample	T_d (°C)	% Weight loss	% Residue
uPPP	569±4	98.04±0.83	1.96±0.83
50:1 dPPP	480±6	86.95±1.10	13.05±1.10

Appendix C Identification of Crystallinity of uPPP and 50:1 dPPP and Structure of Zeolite

X-ray Diffractrometer (Phillips, Rigaku) was used in order to identify the crystallinity of uPPP and 50:1 dPPP and ensure the structure of zeolite. Both uPPP and dPPP powder were compressed into pellet form with 10 mm in diameter and 0.15-0.25 mm in thickness. Zeolite powder was packed into a glass plate. The XRD patterns showed that uPPP had quite high crystalline accompanying with the *d*-spacing value of 4.53, 3.63 and 3.24 Å. The most intense *d*-spacing was 4.53 Å which closely corresponded to the length of a phenyl unit (Kovacic *et al.*, 1963; Marvel *et al.*, 1959). Therefore, it was postulated that the rings were very nearly coplanar. However, the pattern of uPPP did show the existence of some amorphous regions.

Some peaks presenting in the uPPP pattern were disappeared or reduced in intensity after doping with $FeCl_3$ which meant $FeCl_3$ dopant can decease the crystallinity of PPP. It might be due to the distortion of the polymer chain after being doped.

By using XRD technique, the structure and crystallinity ZSM-5 was confirmed. XRD patterns and peak positions matched those observed for the characteristic structure of MFI. The peak intensities and low background lines demonstrated the high crystallinity of the sample.

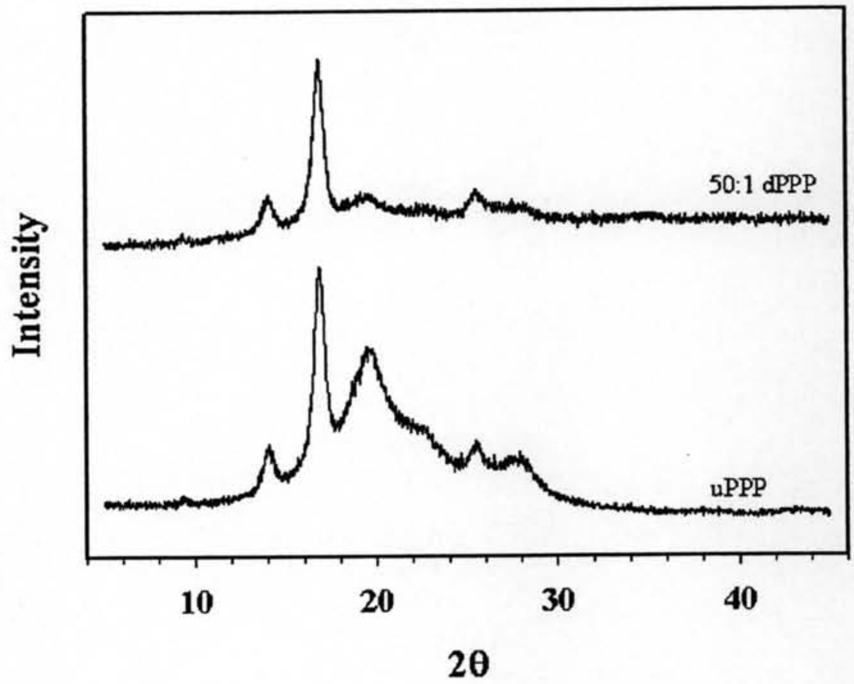

Figure C1 XRD pattern of uPPP and 50:1 dPPP.

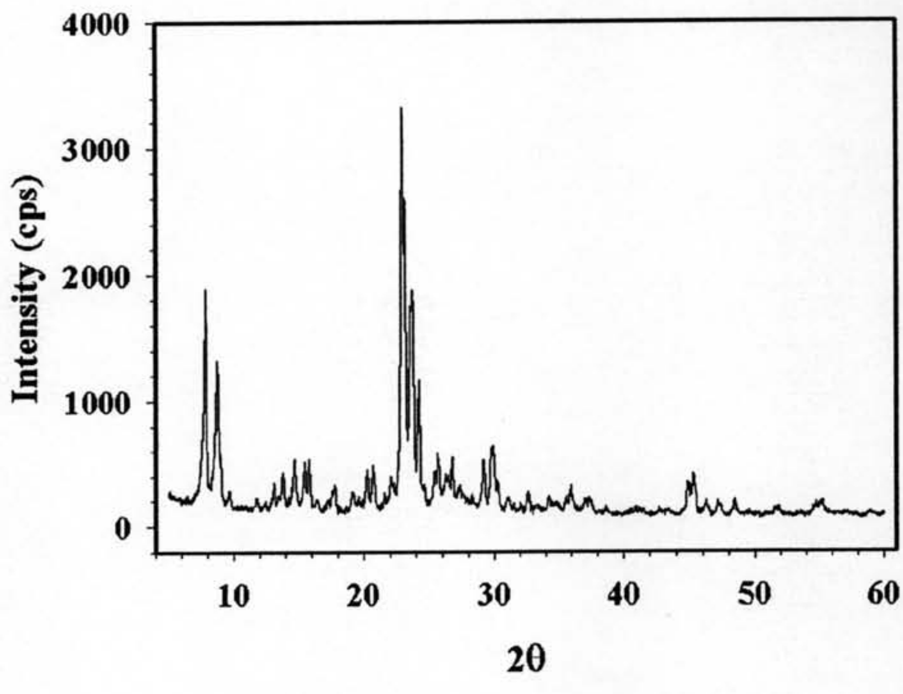

Figure C2 XRD pattern of ZSM-5 with SiO_2/Al_2O_3 of 23.

Appendix D Determination of Particle Size and Particle Size Distribution of PPP and Zeolite Powder

Particle Size Analyser (Malvern/Mastersizer X Version 2.15) was employed to examine the particle size and particle size distribution of materials. Synthesized PPP was ground and subsequently sieved with 54 μm sieve before being analyzed.

Table D1 Mean particle diameter of materials

Materials	Mean particle diameter (μm)				
	1	**2**	**3**	**Avg.**	**SD**
PPP	33.74	33.41	33.69	33.61	0.18
ZSM-5(23)	5.46	5.45	5.47	5.46	0.01

Table D2 Raw data of particle size of uPPP

Particle size diameter (μm)		uPPP					
		1		2		3	
Size low	Size high	In %	Under %	In %	Under %	In %	Under %
0.20	0.48	0.11	0.11	0.11	0.11	0.11	0.11
0.48	0.59	0.33	0.43	0.32	0.43	0.34	0.40
0.59	0.71	0.45	0.88	0.45	0.88	0.47	0.91
0.71	0.86	0.45	1.33	0.44	1.32	0.46	1.37
0.86	1.04	0.34	1.67	0.33	1.65	0.35	1.72
1.04	1.26	0.19	1.86	0.19	1.84	0.20	1.92
1.26	1.52	0.10	1.97	0.10	1.94	0.11	2.03
1.52	1.84	0.12	2.09	0.12	2.06	0.13	2.16
1.84	2.23	0.27	2.36	0.26	2.33	0.27	2.43
2.23	2.70	0.48	2.84	0.48	2.81	0.50	2.93
2.70	3.27	0.68	3.52	0.68	3.49	0.70	3.63
3.27	3.95	0.90	4.42	0.90	4.40	0.93	4.56
3.95	4.79	1.18	5.60	1.18	5.58	1.21	5.77
4.79	5.79	1.51	7.11	1.52	7.09	1.55	7.31
5.79	7.01	1.91	9.03	1.92	9.01	1.95	9.26
7.01	8.48	2.36	11.39	2.36	11.37	2.39	11.66
8.48	10.27	2.86	14.24	2.87	14.25	2.90	14.56
10.27	12.43	3.45	17.70	3.48	17.73	3.51	18.07
12.43	15.05	4.23	21.92	4.29	22.02	4.31	22.38
15.05	18.21	5.32	27.25	5.40	27.42	5.41	27.80
18.21	22.04	6.80	34.06	6.89	34.31	6.87	43.67
22.04	26.68	8.58	42.63	8.66	42.97	8.57	43.23
26.68	32.29	10.34	52.98	10.41	53.38	10.22	53.46
32.29	39.08	11.52	64.49	11.57	64.95	11.32	64.77
39.08	47.30	11.51	75.99	11.53	76.47	11.30	76.06
47.30	57.25	9.83	85.82	9.81	86.28	9.67	85.72
57.25	69.30	7.10	92.93	7.04	93.32	7.00	92.73
69.30	83.87	4.25	97.17	4.15	97.47	4.23	96.96
83.87	101.52	2.06	99.23	1.94	99.42	2.11	99.08
101.52	122.87	0.73	99.97	0.58	100.00	0.82	99.90
122.87	148.72	0.03	100.00	0.00	100.00	0.10	100.00
148.72	180.00	0.00	100.00	0.00	100.00	0.00	100.00

Table D3 Raw data of particle size of ZSM-5(23)

Particle size diameter (μm)		ZSM-5(23)					
		1		2		3	
Size low	Size high	In %	Under %	In %	Under %	In %	Under %
0.05	0.12	0.00	0.00	0.00	0.00	0.00	0.00
0.12	0.15	0.00	0.00	0.00	0.00	0.00	0.00
0.15	0.19	0.00	0.00	0.00	0.00	0.00	0.00
0.19	0.23	0.00	0.00	0.00	0.00	0.00	0.00
0.23	0.28	0.00	0.00	0.00	0.00	0.00	0.00
0.28	0.35	0.00	0.00	0.00	0.00	0.00	0.00
0.35	0.43	0.00	0.00	0.00	0.00	0.00	0.00
0.43	0.53	0.05	0.05	0.05	0.06	0.06	0.06
0.53	0.65	0.30	0.35	0.30	0.36	0.31	0.37
0.65	0.81	0.68	1.03	0.70	1.06	0.71	1.08
0.81	1.00	1.23	2.26	1.25	2.31	1.28	2.35
1.00	1.23	1.92	4.18	1.96	4.27	1.99	4.34
1.23	1.51	2.70	6.88	2.72	6.99	2.73	7.07
1.51	1.86	3.37	10.25	3.36	10.34	3.33	10.40
1.86	2.30	3.84	14.09	3.79	14.14	3.74	14.14
2.30	2.83	4.43	18.52	4.41	18.54	4.40	18.53
2.83	3.49	6.12	24.66	6.17	24.73	6.25	24.79
3.49	4.30	9.35	34.00	9.47	34.19	9.60	34.38
4.30	5.29	14.17	48.19	14.25	48.45	14.25	48.64
5.29	6.52	18.51	66.67	18.37	66.80	18.05	66.67
6.52	8.04	17.38	84.04	17.17	83.96	16.84	83.49
8.04	9.91	10.69	94.71	10.66	94.60	10.74	94.21
9.91	12.21	4.27	99.01	4.35	98.98	4.60	98.85
12.21	15.04	0.98	100.00	1.02	100.00	1.14	100.00
15.04	18.54	0.00	100.00	0.00	100.00	0.00	100.00
18.54	22.84	0.00	100.00	0.00	100.00	0.00	100.00
22.84	28.15	0.00	100.00	0.00	100.00	0.00	100.00
28.15	34.69	0.00	100.00	0.00	100.00	0.00	100.00
34.69	42.75	0.00	100.00	0.00	100.00	0.00	100.00
42.75	52.68	0.00	100.00	0.00	100.00	0.00	100.00
52.68	64.92	0.00	100.00	0.00	100.00	0.00	100.00
64.92	80.00	0.00	100.00	0.00	100.00	0.00	100.00

Appendix E Density Measurement

Density of PPP and zeolite can be measured by using pycnometer at controlled temperature. Blank pycnometer was firstly weighed and then water was added into the pycnometer and weight of pycnometer with water was measured again. The density of water can be calculated through equation (E1)

$$\rho_w = \frac{(a-b)}{25} \tag{E1}$$

where ρ_w is the density of water (g.cm^{-3}), a is the weight of pycnometer with water (g), b is the weight of blank pycnometer (g).

The blank pycnometer was weighed again and then sample powder was introduced into the pycnometer and the total weight was measured. After that the water was added into the same pycnometer and again the total weight was measured. In this step, the volume of added water will be obtained from equation (E2) and finally the density of the sample can be calculated through equation (E3)

$$A = \frac{(e-d)}{\rho_w} \tag{E2}$$

where A is the volume of added water (cm^3), e is the weight of pycnometer with sample and added water (g), d is the weight of pycnometer with sample (g).

$$\rho_m = \frac{(d-b)}{25-A} \tag{E3}$$

where ρ_m is the density of matarial (g.cm^{-3}).

Table E1 Density of materials

Materials	Density(g.cm^{-3})
PPP	1.3273±0.0011
ZSM-5(23)	1.9739±0.0004

Appendix F Morphology

Scanning Electron Microscope (SEM) (JEOL/JSM 5200) was utilized to examine the morphology of materials. Samples were coated with gold before being characterized in order to suppress the charge up phenomena. The morphology of PPP (Figure F-1) shows rough surface and irregular shapes.

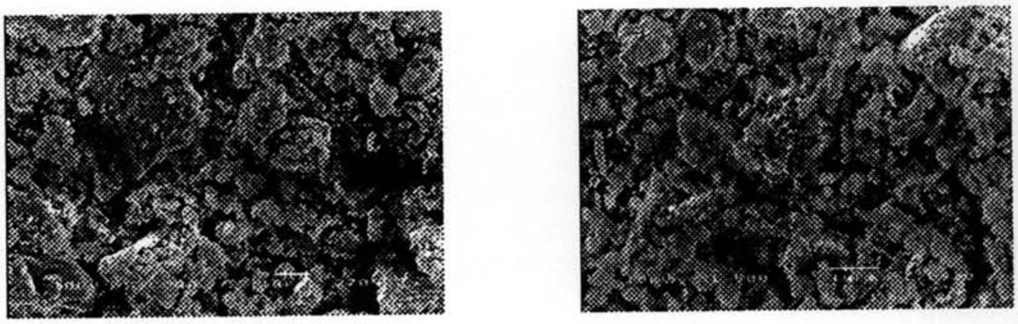

(a) (b)

Figure F1 Morphology of PPP at magnifications of (a) 1000; (b) 1500.

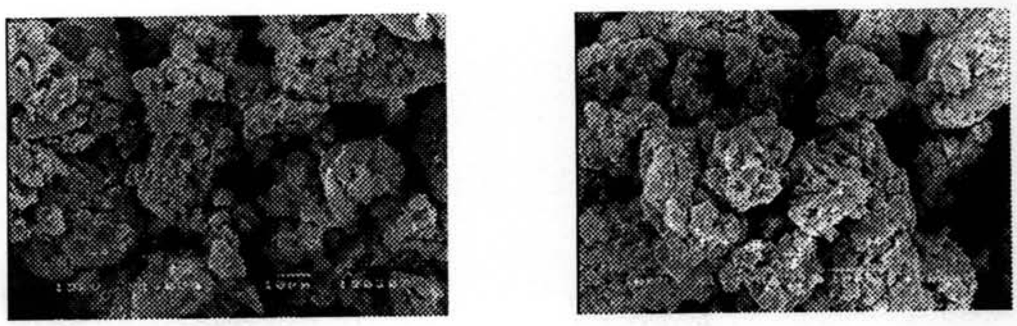

(a) (b)

Figure F2 Morphology of dPPP at magnifications of (a) 1000; (b) 1500.

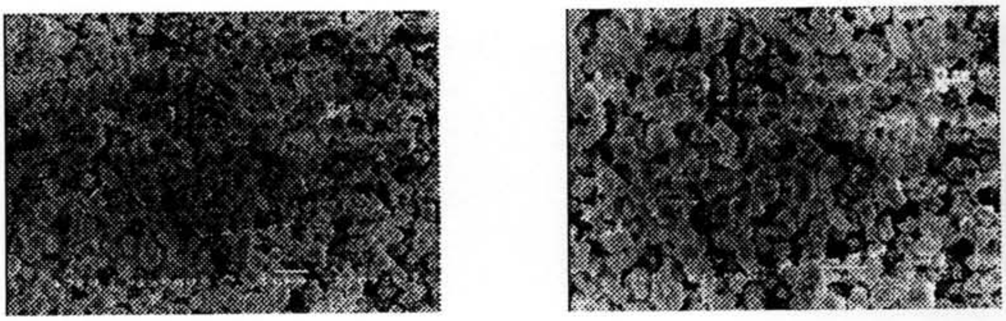

(a) (b)

Figure F3 Morphology of ZSM-5(23) at magnifications of (a) 1000; (b) 1500.

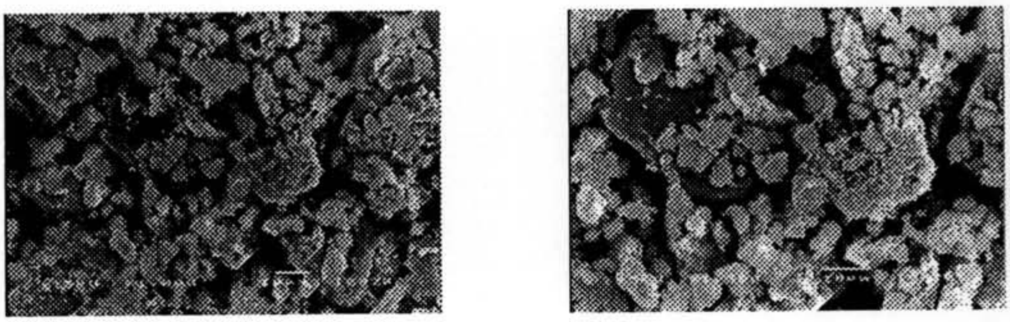

(a) (b)

Figure F4 Morphology of dPPP(90)/NaZ23 at magnifications of (a) 1000; (b) 1500.

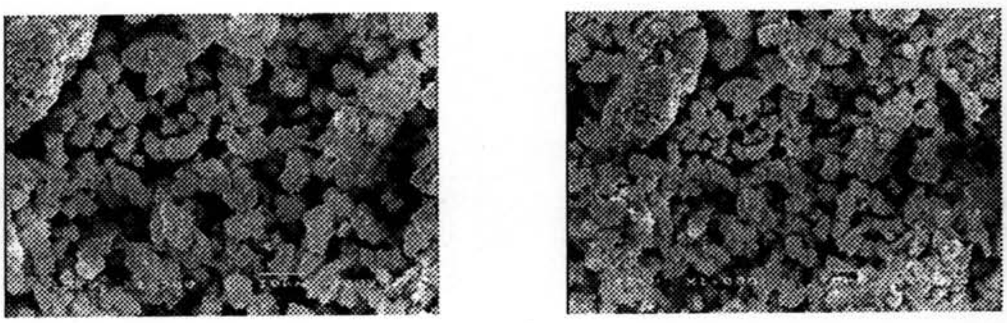

(a) (b)

Figure F5 Morphology of dPPP(80)/NaZ23 at magnifications of (a) 1000; (b) 1500.

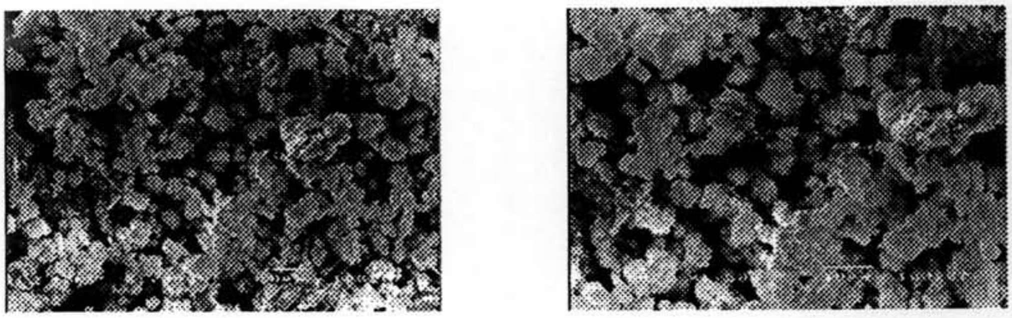

(a) (b)

Figure F6 Morphology of dPPP(70)/NaZ23 at magnifications of (a) 1000; (b) 1500.

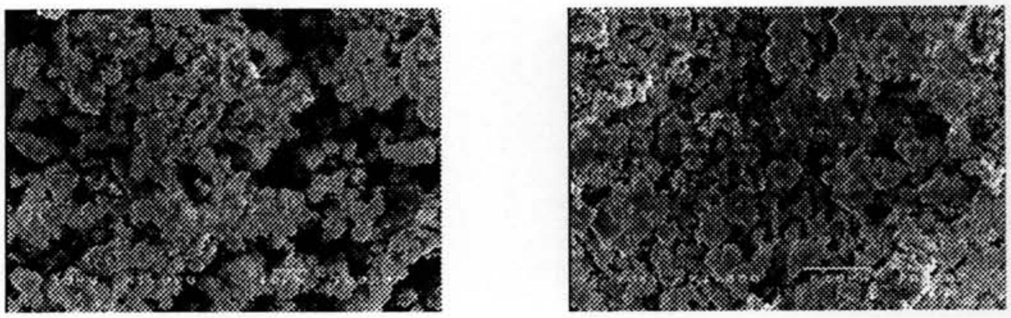

(a) (b)

Figure F7 Morphology of dPPP(70)/NaZ23 at magnifications of (a) 1000; (b) 2000.

Appendix G Identification of Si/Al and Cation Exchange Level of Zeolite

An Atomic Absorption Spectrometer (AAS) (Varian/SpectrAA 300) was used to determine the amount of Si and Al containing in zeolite and the amount of desired cation after ion exchange processes. The known weight zeolite was dissolved with hydrofluoric acid (HF) and hydrochloric acid (HCl). After the volume of solution was adjusted, the solution was filtered before being tested. Standard, blank and sample solutions were prepared for testing of each cation and different lamps were used for different cations.

The Si/Al ratio of zeolite can be calculated via equation (G1)

$$Si/Al\ ratio = \frac{mole\ of\ Si/g\ of\ zeolite}{mole\ of\ Al/g\ of\ zeolite} \tag{G1}$$

Table G1 Si/Al ratios of zeolite

Zeolite	Cation content (mole/g zeolite)		Si/Al
	Si	Al	
ZSM-5(23)	1.3849×10^{-2}	1.0930×10^{-3}	12.67

Before performing cation exchange process, ZSM-5 zeolite contains the NH_4^+ cation. After the process, cation containing in the ZSM-5 was changed and the actual amount of balancing cation was then determined. Cation exchange level can be calculated on the assumption that 100% cation exchange possesses identical mole number of incoming cation and Al as followed equation (G-2)

$$Cation\ exchange\ level = \frac{mole\ of\ cation/g\ of\ zeolite}{mole\ of\ Al/g\ of\ zeolite} \tag{G-2}$$

Table G2 The cation exchange level of NH_4ZSM-5(23) with Na^+ and K^+

Sample	Cation	Times	$[Al_3^+]$ (mmol/g zeolite)	[cation] (mmol/g zeolite)	% Exchange
ZSM-5(23)	Na^+	1st	1.0978	1.0674	97.23
	K^+	1st	1.0978	1.0576	96.34

Appendix H Surface Area and Pore Volume of Zeolite

Surface area and pore volume of zeolite were determined by employing a Surface Area Analyzer (SAA) (Quantachrome/Autosorb-1). Dried zeolite was weighed and out gassed at 250 °C over night before being performed adsorption and desorption with He and N_2 gases.

Table H1 Surface area and pore volume of zeolite

Zeolite	BET Surface area (m^2/g)	Pore volume (cm^3/g)
NH_4ZSM-5(23)	290.1±0.85	0.1819±0.0031
HZSM-5(23)	332.6±6.51	0.2075±0.0006
NaZSM-5(23)	283.1±8.63	0.1759±0.0112
KZSM-5(23)	273.3±1.34	0.1663±0.0074

It was well-known that if the zeolite contains different cation, the surface area and pore volume of the zeolite are also different due to the various types of cation whose size of cation are not the same. From table G-1, the surface area and pore volume of ammonium cation form existing in ZSM-5 are 290.1m^2/g and 0.1819 cm^3/g, respectively. After calcination without passing cation exchanged process, ammonium cation became H^+ because of the removal of NH_3 during calcination process, therefore the surface are and pore volume of zeolite increase up to 332.6 m^2/g and 0.2075 cm^3/g, respectively. Due to K^+ possesses the larger cation size than Na^+, thus ZSM-5 containing K^+ have less surface area and pore volume than NaZSM-5.

Appendix I Correction Factor (K) Measurement

A two point probe meter connected with a source power supplier (Keithley/ Model 6517A) was employed to determine the electrical conductivity of materials. A constant voltage is applied and a current is simultaneously measured.

According to the geometric effects of the probe, the geometrical correction factor was taken, depending on the configuration and probe tip spacing

$$K = \frac{w}{l} \tag{I1}$$

where K is geometric correction factor, w is width of probe tip spacing (cm), l is length between probes (cm).

The constant K can be determined by using standard materials whose specific resistivity values are known. In our case, silicon wafer chips were used as the standard materials. The resistance was measured by using our custom made two-point probe, obtained by applying various voltages and simultaneously measuring currents. The geometric correction factor was calculated via equation (I2)

$$K = \frac{\rho}{R \times t} = \frac{I \times \rho}{V \times t} \tag{I2}$$

where ρ is resistivity of standard silicon wafer (Ω.cm), which was calibrated by using four point probe at Thailand Microelectronic Centre (TMEC), R is resistance of film (Ω.), t is film thickness (cm), I is measured current (A) and V is applied voltage (V).

Table I1 The correction factor of several two point probes.

Probe	Correction Factor (K)				
	1	**2**	**3**	**Avg.**	**SD**
1	3.05E-05	2.785E-05	7.445E-06	2.195E-05	1.902E-06
2	7.422E-05	9.872E-06	4.200E-05	4.205E-05	4.550E-05
3	1.506E-05	4.847E-05	3.180E-05	3.177E-05	2.362E-05
4	8.063E-06	8.213E-06	8.260E-06	8.178E-06	1.028E-07
5	2.385E-05	2.221E-05	2.755E-05	2.454E-05	2.735E-06
6	3.501E-05	3.453E-05	3.488E-05	3.481E-05	2.495E-07

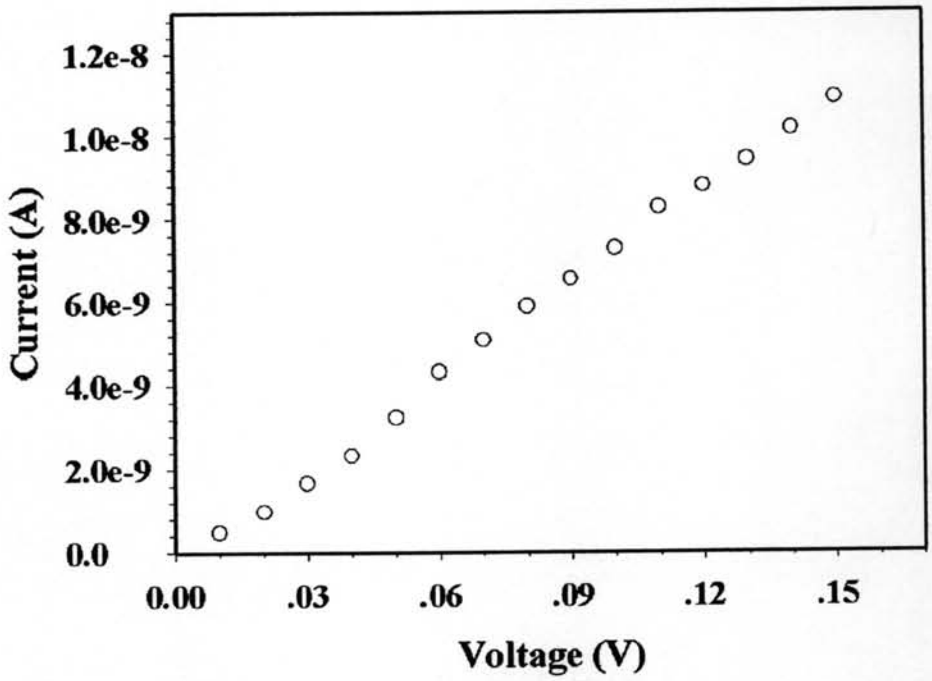

Figure I1 Voltage vs. current data of the probe calibration with Si-wafer whose sheet resistivity of 107.373 Ω/sq, at 24-25 °C, 50-60 %RH.

Table I2 Voltage-current data of the probe 1 calibration with Si-wafer whose sheet resistivity of 107.373 Ω/sq, at 24-25 °C, 50-60 %RH

Applied Voltage (V)			Current (A)		
1	**2**	**3**	**1**	**2**	**3**
0.01	0.01	0.01	5.80E-10	4.48E-10	4.25E-10
0.02	0.02	0.02	1.16E-09	8.97E-10	8.51E-10
0.03	0.03	0.03	1.70E-09	1.60E-09	1.64E-09
0.04	0.04	0.04	2.24E-09	2.30E-09	2.43E-09
0.05	0.05	0.05	3.28E-09	3.17E-09	3.25E-09
0.06	0.06	0.06	4.23E-09	4.32E-09	4.39E-09
0.07	0.07	0.07	5.06E-09	5.08E-09	5.09E-09
0.08	0.08	0.08	6.13E-09	5.96E-09	5.60E-09
0.09	0.09	0.09	6.63E-09	6.61E-09	6.42E-09
0.10	0.10	0.10	7.28E-09	7.28E-09	7.34E-09
0.11	0.11	0.11	8.33E-09	8.25E-09	8.25E-09
0.12	0.12	0.12	8.90E-09	8.75E-09	8.71E-09
0.13	0.13	0.13	9.48E-09	9.36E-09	9.42E-09
0.14	0.14	0.14	1.02E-08	1.01E-08	1.02E-08
0.15	0.15	0.15	1.10E-08	1.07E-08	1.10E-08

Table I3 Voltage-current data of the probe 2 calibration with Si-wafer whose sheet resistivity of 107.373 Ω/sq, at 24-25 °C, 50-60 %RH

Applied Voltage (V)			Current (A)		
1	**2**	**3**	**1**	**2**	**3**
0.05	0.05	0.05	3.64E-08	3.49E-08	3.40E-08
0.10	0.10	0.10	7.17E-08	7.10E-08	6.66E-08
0.15	0.15	0.15	1.00E-07	9.98E-08	1.00E-07
0.20	0.20	0.20	1.33E-07	1.27E-07	1.22E-07
0.25	0.25	0.25	1.62E-07	1.64E-07	1.50E-07
0.30	0.30	0.30	1.93E-07	1.94E-07	1.89E-07
0.35	0.35	0.35	2.38E-07	2.40E-07	2.39E-07
0.40	0.40	0.40	2.87E-07	2.79E-07	2.78E-07
0.45	0.45	0.45	3.23E-07	3.23E-07	3.12E-07
0.50	0.50	0.50	3.63E-07	3.65E-07	3.53E-07
0.55	0.55	0.55	4.01E-07	3.95E-07	3.85E-07
0.60	0.60	0.60	4.35E-07	4.34E-07	4.30E-07
0.65	0.65	0.65	4.85E-07	4.78E-07	4.73E-07
0.70	0.70	0.70	5.04E-07	4.99E-07	4.94E-07

Table I4 Voltage-current data of the probe 3 calibration with Si-wafer whose sheet resistivity of 107.373 Ω/sq, at 24-25 °C, 50-60 %RH

Applied Voltage (V)			Current (A)		
1	2	3	1	2	3
0.05	0.05	0.05	5.91E-09	5.89E-09	6.01E-09
0.10	0.10	0.10	1.45E-08	1.42E-08	1.40E-08
0.15	0.15	0.15	2.36E-08	2.31E-08	2.29E-08
0.20	0.20	0.20	3.16E-08	3.02E-08	2.98E-08
0.25	0.25	0.25	3.72E-08	3.63E-08	3.59E-08
0.30	0.30	0.30	4.38E-08	4.22E-08	4.19E-08
0.35	0.35	0.35	4.94E-08	4.80E-08	4.81E-08
0.40	0.40	0.40	5.61E-08	5.51E-08	5.48E-08
0.45	0.45	0.45	6.14E-08	6.08E-08	6.08E-08
0.50	0.50	0.50	6.80E-08	6.76E-08	6.76E-08
0.55	0.55	0.55	7.54E-08	7.38E-08	7.36E-08
0.60	0.60	0.60	8.14E-08	8.22E-08	8.12E-08
0.65	0.65	0.65	9.09E-08	9.18E-08	9.12E-08
0.70	0.70	0.70	1.04E-07	1.03E-07	1.03E-07

Table I5 Voltage-current data of the probe 4 calibration with Si-wafer whose sheet resistivity of 107.373 Ω/sq, at 24-25 °C, 50-60 %RH

Applied Voltage (V)			Current (A)		
1	2	3	1	2	3
0.01	0.01	0.01	8.74E-10	8.41E-10	8.68E-10
0.02	0.02	0.02	1.09E-09	1.06E-09	1.05E-09
0.03	0.03	0.03	1.33E-09	1.40E-09	1.33E-09
0.04	0.04	0.04	2.54E-09	2.58E-09	2.54E-09
0.05	0.05	0.05	3.07E-09	3.07E-09	3.26E-09
0.06	0.06	0.06	4.83E-09	4.87E-09	5.22E-09
0.07	0.07	0.07	5.32E-09	5.43E-09	5.28E-09
0.08	0.08	0.08	6.14E-09	6.39E-09	6.62E-09
0.09	0.09	0.09	7.83E-09	8.03E-09	7.63E-09
0.10	0.10	0.10	8.62E-09	8.75E-09	8.24E-09
0.11	0.11	0.11	9.58E-09	8.91E-09	8.85E-09
0.12	0.12	0.12	9.52E-09	9.69E-09	9.65E-09
0.13	0.13	0.13	1.11E-08	1.15E-08	1.26E-08
0.14	0.14	0.14	1.35E-08	1.34E-08	1.38E-08
0.15	0.15	0.15	1.39E-08	1.42E-08	1.43E-08

Table I6 Voltage-current data of the probe 5 calibration with Si-wafer whose sheet resistivity of 107.373 Ω/sq, at 24-25 °C, 50-60 %RH

Applied Voltage (V)			Current (A)		
1	2	3	1	2	3
0.005	0.005	0.005	7.03E-10	5.68E-10	9.56E-10
0.01	0.01	0.01	2.33E-09	2.22E-09	2.52E-09
0.02	0.02	0.02	3.98E-09	4.32E-09	6.68E-09
0.03	0.03	0.03	7.16E-09	6.70E-09	6.68E-09
0.04	0.04	0.04	9.36E-09	8.15E-09	9.38E-09
0.05	0.05	0.05	1.44E-08	1.31E-08	1.53E-08

Table I7 Voltage-current data of the probe 6 calibration with Si-wafer whose sheet resistivity of 107.373 Ω/sq, at 24-25 °C, 50-60 %RH

Applied Voltage (V)			Current (A)		
1	2	3	1	2	3
0.005	0.005	0.005	1.20E-09	1.24E-09	1.31E-09
0.010	0.010	0.010	3.85E-09	3.61E-09	3.65E-09
0.015	0.015	0.015	4.75E-09	4.85E-09	5.01E-09
0.020	0.020	0.020	5.97E-09	6.03E-09	5.82E-09
0.025	0.025	0.025	7.07E-09	7.13E-09	7.37E-09
0.030	0.030	0.030	9.63E-09	9.69E-09	9.72E-09
0.035	0.035	0.035	1.24E-08	1.23E-08	1.29E-08
0.040	0.040	0.040	1.42E-08	1.39E-08	1.42E-08
0.045	0.045	0.045	1.72E-08	1.59E-08	1.47E-08

Appendix J Conductivity Measurement

The electrical conductivity (σ) can be measured by using the two-point probe mater connected with a voltage supplier (Keithley, 6517A) which its constant voltage can be changed and the current is reported. The conductivity measurement was performed under atmospheric pressure, 40-60% RH and at 25-27 °C. The responsive current linearly proportional to the applied voltage is called the linear ohmic regime which can be identified by plotting the applied voltage against with the current. The voltage and the current in the regime were converted to the electrical conductivity by following equation (J1)

$$\sigma = \frac{1}{\rho} = \frac{1}{R_s \, x \, t} = \frac{I}{K \, x \, V \, x \, t} \qquad \text{(J1)}$$

where σ is specific conductivity (S/cm), ρ is specific resistivity (Ω.cm), R_s is sheet resistance (Ω/sq), t is thickness of sample pellet (cm), V is applied voltage (voltage drop) (V), I is measured current (A), and K is geometric correction factor of the two-point probe meter.

In this measurement, the probe 2 was used; whose K is 4.205 $x10^{-5}$ and the thickness of the samples was measured by using a thickness gauge.

Table J1 The specific conductivity (S/cm) of uPPP, dPPP with various doping level and NaZSM-5(23) zeolite

Sample	Specific conductivity (S/cm)
uPPP	(1.171±0.073)E-05
10:1 dPPP	(1.260±0.248)E-04
20:1 dPPP	(2.214±1.140)E-02
50:1 dPPP	(8.701±4.246)E-01
100:1 dPPP	(1.481±0.733)E+00
NaZSM-5(23)	(8.670±2.543)E-03

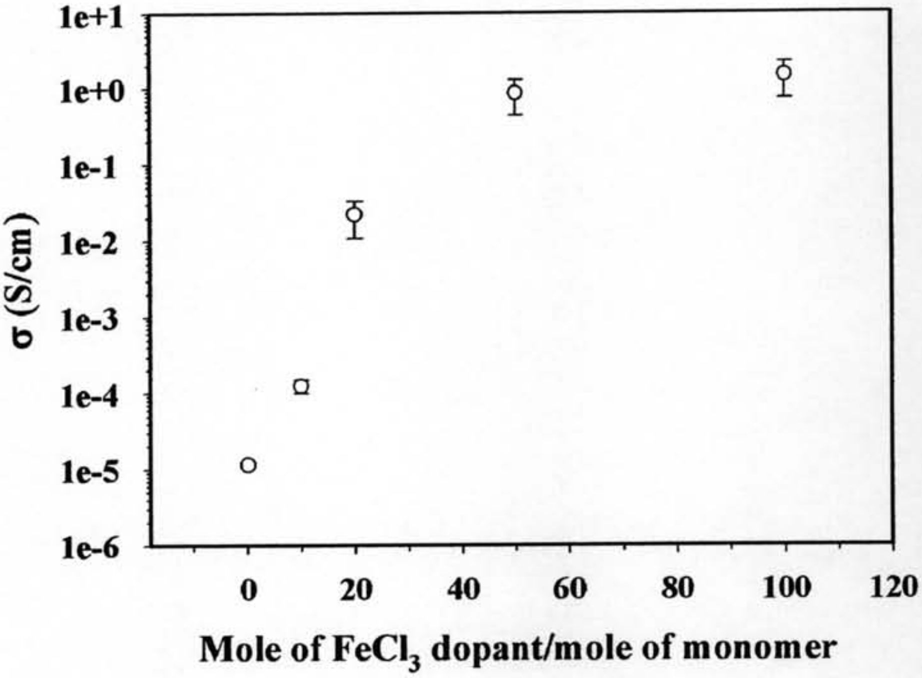

Figure J1 The specific conductivity of dPPP at various mole ratios between dopant and monomer at 24-25 °C, 50-60 %RH.

Table J2 Voltage-current data in linear regime of uPPP at 24-25 °C, 50-60 %RH

Applied voltage (V)			Measure current (A)			Conductivity (S/cm)		
1	2	3	1	2	3	1	2	3
0.2	0.2	0.2	1.50E-12	1.57E-12	1.63E-12	8.59E-06	9.02E-06	9.37E-06
0.4	0.4	0.4	3.66E-12	3.58E-12	3.55E-12	1.05E-05	1.03E-05	1.02E-05
0.6	0.6	0.6	5.86E-12	6.20E-12	5.98E-12	1.12E-05	1.19E-05	1.14E-05
0.8	0.8	0.8	8.58E-12	8.22E-12	8.22E-12	1.23E-05	1.18E-05	1.18E-05
1.0	1.0	1.0	1.05E-11	1.05E-11	1.04E-11	1.21E-05	1.21E-05	1.19E-05
1.2	1.2	1.2	1.25E-11	1.26E-11	1.24E-11	1.19E-05	1.20E-05	1.18E-05
1.4	1.4	1.4	1.42E-11	1.42E-11	1.42E-11	1.17E-05	1.17E-05	1.17E-05
1.6	1.6	1.6	1.57E-11	1.58E-11	1.58E-11	1.13E-05	1.13E-05	1.13E-05
1.8	1.8	1.8	1.78E-11	1.78E-11	1.75E-11	1.13E-05	1.13E-05	1.12E-05
2.0	2.0	2.0	1.92E-11	1.88E-11	1.88E-11	1.10E-05	1.08E-05	1.08E-05

Table J3 Voltage-current data in linear regime of 10:1 dPPP at 24-25 °C, 50-60 %RH

Applied voltage (V)			Measure current (A)			Conductivity (S/cm)		
1	2	3	1	2	3	1	2	3
0.1	0.1	0.1	9.30E-12	1.04E-11	1.08E-11	1.31E-04	1.47E-04	1.53E-04
0.2	0.2	0.2	1.87E-11	1.82E-11	1.82E-11	1.32E-04	1.29E-04	1.29E-04
0.3	0.3	0.3	2.87E-11	2.83E-11	2.82E-11	1.35E-04	1.33E-04	1.33E-04
0.4	0.4	0.4	3.75E-11	3.72E-11	3.72E-11	1.32E-04	1.31E-04	1.31E-04
0.5	0.5	0.5	4.62E-11	4.55E-11	4.51E-11	1.31E-04	1.29E-04	1.28E-04
0.6	0.6	0.6	5.45E-11	5.39E-11	5.38E-11	1.29E-04	1.27E-04	1.27E-04
0.7	0.7	0.7	6.28E-11	6.29E-11	6.20E-11	1.27E-04	1.27E-04	1.25E-04
0.8	0.8	0.8	7.13E-11	7.13E-11	7.07E-11	1.26E-04	1.26E-04	1.25E-04
0.9	0.9	0.9	7.99E-11	7.88E-11	7.90E-11	1.26E-04	1.24E-04	1.24E-04
1.0	1.0	1.0	8.82E-11	8.82E-11	8.75E-11	1.25E-04	1.25E-04	1.24E-04
1.1	1.1	1.1	9.71E-11	9.59E-11	9.55E-11	1.37E-04	1.23E-04	1.23E-04

Table J4 Voltage-current data in linear regime of 20:1 dPPP at 24-25 °C, 50-60 %RH

Applied voltage (V)			Measured current (A)			Conductivity (S/cm)		
1	2	3	1	2	3	1	2	3
1	1	1	2.41E-09	2.23E-09	1.81E-09	3.51E-03	3.25E-03	2.63E-03
2	2	2	8.85E-09	8.47E-09	7.99E-09	6.44E-03	6.17E-03	5.82E-03
3	3	3	1.60E-08	1.58E-08	1.55E-08	7.76E-03	7.66E-03	7.55E-03
4	4	4	2.47E-08	2.44E-08	2.43E-08	9.01E-03	8.89E-03	8.85E-03
5	5	5	3.46E-08	3.44E-08	3.42E-08	1.01E-02	1.00E-02	9.97E-03
6	6	6	4.51E-08	4.48E-08	4.47E-08	1.10E-02	1.09E-02	1.08E-02
7	7	7	5.55E-08	5.53E-08	5.50E-08	1.16E-02	1.15E-02	1.14E-02
8	8	8	6.62E-08	6.58E-08	6.55E-08	1.21E-02	1.20E-02	1.19E-02
9	9	9	7.68E-08	7.68E-08	7.68E-08	1.24E-02	1.24E-02	1.24E-02
10	10	10	8.88E-08	8.94E-08	8.85E-08	1.29E-02	1.30E-02	1.29E-02

Table J5 Voltage-current data in linear regime of 50:1 dPPP at 24-25 °C, 50-60 %RH

Applied voltage (V)			Measured current (A)			Conductivity (S/cm)		
1	2	3	1	2	3	1	2	3
0.1	0.1	0.1	1.11E-08	1.09E-08	1.08E-08	0.111813	0.109453	0.108562
0.2	0.2	0.2	3.37E-08	3.28E-08	3.14E-08	0.169619	0.164998	0.158225
0.3	0.3	0.3	5.37E-08	5.44E-08	5.27E-08	0.180072	0.182382	0.176912
0.4	0.4	0.4	7.51E-08	7.29E-08	6.91E-08	0.188950	0.183487	0.173976
0.5	0.5	0.5	9.07E-08	8.98E-08	8.87E-08	0.182579	0.180773	0.178435
0.6	0.6	0.6	1.11E-07	1.10E-07	1.06E-07	0.186147	0.184265	0.178023
0.7	0.7	0.7	1.24E-07	1.19E-07	1.19E-07	0.177664	0.171037	0.170959
0.8	0.8	0.8	1.41E-07	1.43E-07	1.42E-07	0.176984	0.179755	0.178662
0.9	0.9	0.9	1.55E-07	1.59E-07	1.54E-07	0.173118	0.177641	0.171850
1.0	1.0	1.0	1.70E-07	1.64E-07	1.57E-07	0.171437	0.164798	0.157886

Table J6 Voltage-current data in linear regime of 100:1 dPPP at 24-25 °C, 50-60 %RH

Applied voltage (V)			Measured current (A)			Conductivity (S/cm)		
1	2	3	1	2	3	1	2	3
0.1	0.1	0.1	1.02E-07	1.03E-07	1.05E-07	0.972079	0.983163	1.000698
0.2	0.2	0.2	2.51E-07	2.58E-07	2.63E-07	1.196080	1.232245	1.254015
0.3	0.3	0.3	4.13E-07	4.2E-07	4.44E-07	1.313635	1.335709	1.413778
0.4	0.4	0.4	6.38E-07	6.36E-07	6.41E-07	1.522853	1.517735	1.529188
0.5	0.5	0.5	8.77E-07	8.97E-07	9.06E-07	1.673749	1.712993	1.729517
0.6	0.6	0.6	1.20E-06	1.25E-06	1.27E-06	1.905577	1.990477	2.026039
0.7	0.7	0.7	1.63E-06	1.65E-06	1.69E-06	2.216643	2.256428	2.306414
0.8	0.8	0.8	1.98E-06	1.93E-06	1.95E-06	2.364017	2.307162	2.326751
0.9	0.9	0.9	2.27E-06	2.3E-06	2.35E-06	2.406210	2.436363	2.490092
1.0	1.0	1.0	2.66E-06	2.63E-06	2.61E-06	2.542574	2.515294	2.494274

Table J7 Voltage-current data in linear regime of NaZSM-5(23) at 24-25 °C, 50-60 %RH

Applied voltage (V)			Measured current (A)			Conductivity (S/cm)		
1	2	3	1	2	3	1	2	3
0.5	0.5	0.5	3.77E-09	2.13E-09	3.77E-09	5.64E-03	1.79E-03	3.23E-03
1.0	1.0	1.0	1.37E-08	5.46E-09	1.37E-08	1.03E-02	2.29E-03	5.26E-03
1.5	1.5	1.5	2.25E-08	9.99E-09	2.25E-08	1.12E-02	2.80E-03	5.93E-03
2.0	2.0	2.0	3.14E-08	1.78E-08	3.14E-08	1.17E-02	3.74E-03	6.74E-03
2.5	2.5	2.5	4.02E-08	2.98E-08	4.02E-08	1.20E-02	4.99E-03	7.66E-03
3.0	3.0	3.0	4.78E-08	3.9E-08	4.78E-08	1.19E-02	5.46E-03	7.92E-03
3.5	3.5	3.5	5.55E-08	4.36E-08	5.55E-08	1.18E-02	5.23E-03	7.76E-03
4.0	4.0	4.0	6.34E-08	5.31E-08	6.34E-08	1.18E-02	5.57E-03	7.97E-03
4.5	4.5	4.5	7.14E-08	5.9E-08	7.14E-08	1.18E-02	5.51E-03	7.93E-03
5.0	5.0	5.0	8.01E-08	8.07E-08	8.01E-08	1.20E-02	6.78E-03	8.81E-03
5.5	5.5	5.5	8.78E-08	1.06E-07	8.78E-08	1.19E-02	8.12E-03	9.66E-03
6.0	6.0	6.0	9.67E-08	1.15E-07	9.67E-08	1.20E-02	8.06E-03	9.67E-03
6.5	6.5	6.5	1.04E-07	1.32E-07	1.04E-07	1.20E-02	8.50E-03	9.94E-03
7.0	7.0	7.0	1.12E-07	1.44E-07	1.12E-07	1.19E-02	8.60E-03	9.99E-03
7.5	7.5	7.5	1.17E-07	1.43E-07	1.17E-07	1.17E-02	8.02E-03	9.51E-03
8.0	8.0	8.0	1.23E-07	1.62E-07	1.23E-07	1.15E-02	8.50E-03	9.75E-03
8.5	8.5	8.5	1.31E-07	1.62E-07	1.31E-07	1.15E-02	8.01E-03	9.44E-03
9.0	9.0	9.0	1.41E-07	1.76E-07	1.41E-07	1.17E-02	8.19E-03	9.64E-03
9.5	9.5	9.5	1.47E-07	1.92E-07	1.47E-07	1.16E-02	8.48E-03	9.78E-03
10.0	10.0	10.0	1.53E-07	1.91E-07	1.53E-07	1.15E-02	8.02E-03	9.43E-03

Appendix K Electrical Conductivity Sensitivity Measurement

The electrical conductivity of dPPP and dPPP/zeolite composite pellets under both N_2 and NH_3 gas atmosphere were carried out by using two point probe, under pressure 1 atm, at 29±1 °C. The electrical conductivity response of the sample is defined as the difference between the equilibrium conductivity of sample under exposed to NH_3 and that of samples under N_2 exposure.

$$\Delta\sigma = \sigma_{NH_3} - \sigma_{N_2\, inotial} \tag{K1}$$

The electrical conductivity sensitivity is calculated from the electrical conductivity response divided by equilibrium conductivity under exposed to N_2.

$$Sensitivity = \Delta\sigma / \sigma_{N_2\, initial} \tag{K2}$$

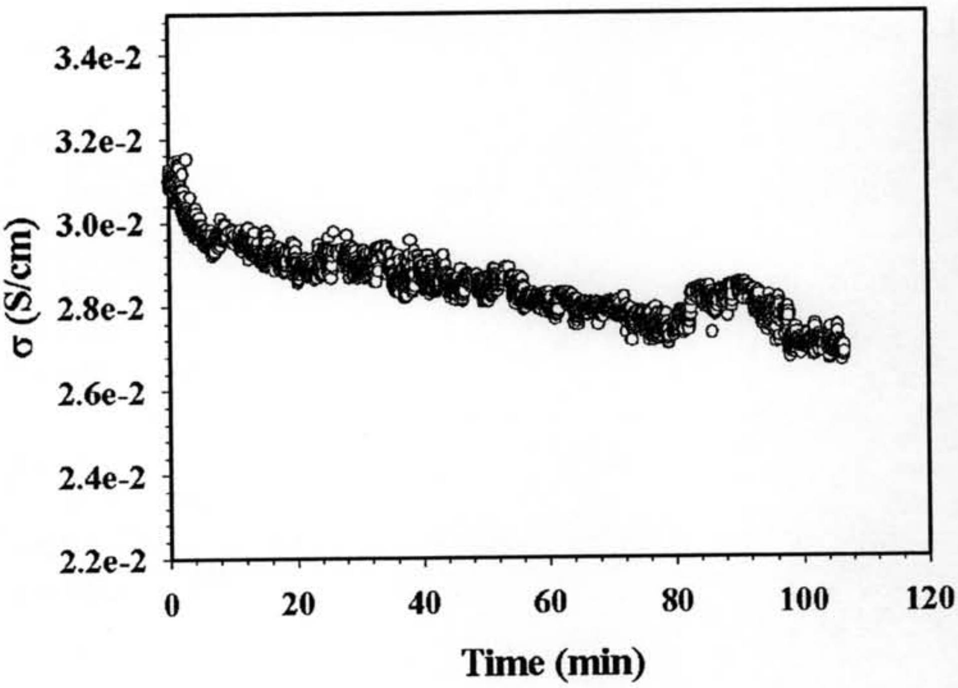

Figure K1 Specific conductivity of 50:1 dPPP when exposed to 0.15625%v NH_3.

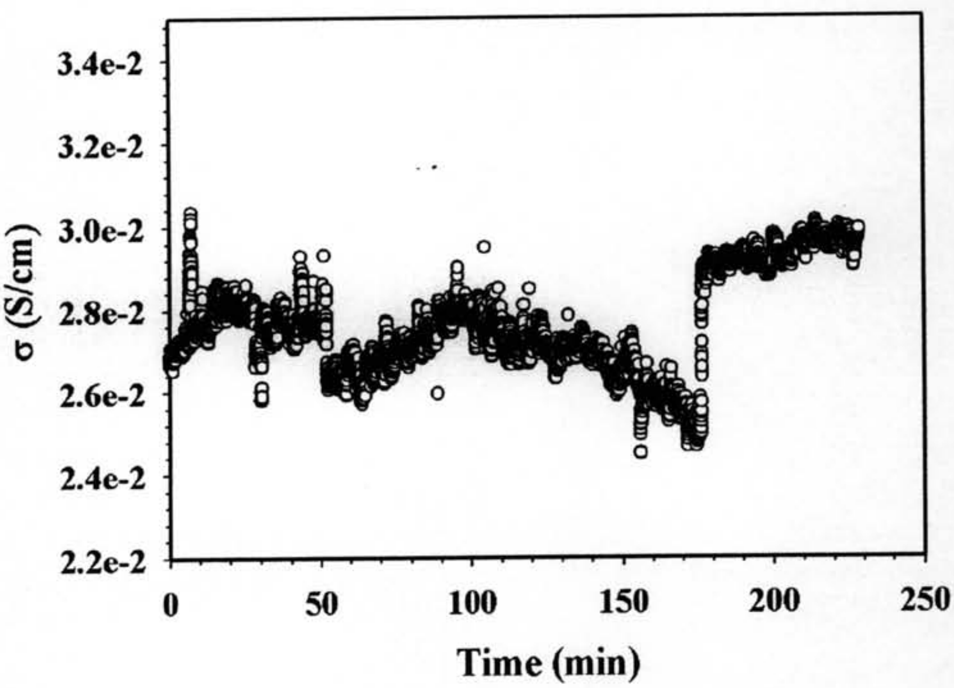

Figure K2 Specific conductivity of 50:1 dPPP after evacuating 0.15625%v NH_3 and exposed to N_2.

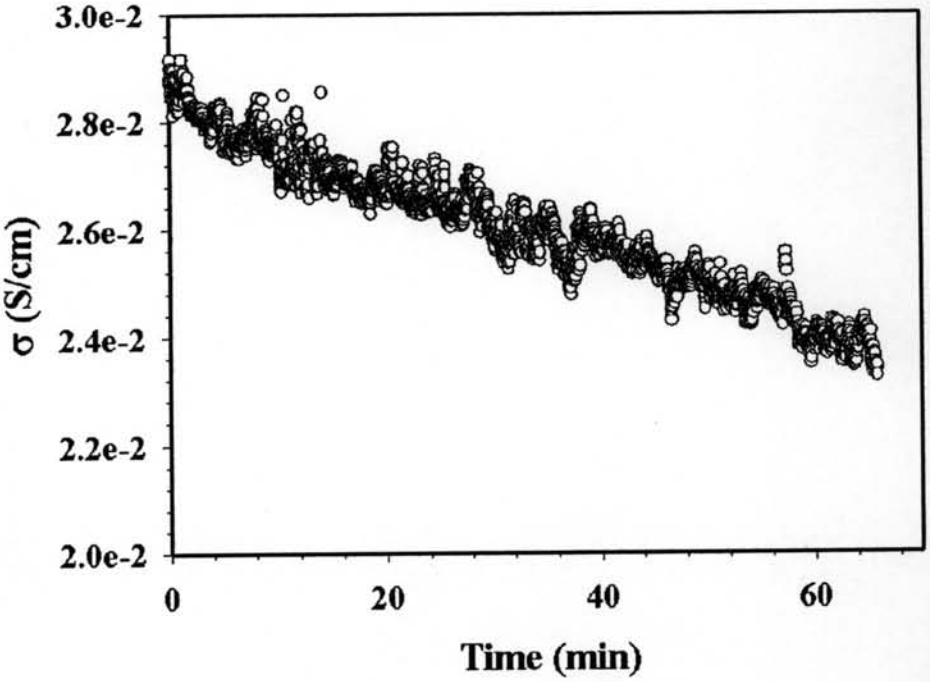

Figure K3 Specific conductivity of 50:1 dPPP when exposed to 0.3125%v NH_3.

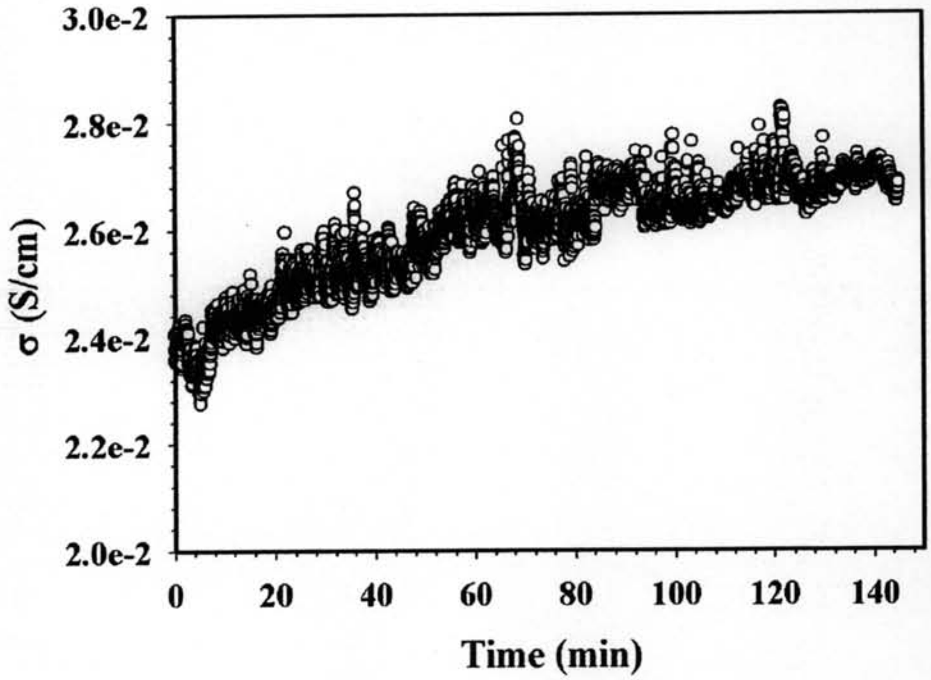

Figure K4 Specific conductivity of 50:1 dPPP after evacuating 0.3125%v NH_3 and exposed to N_2.

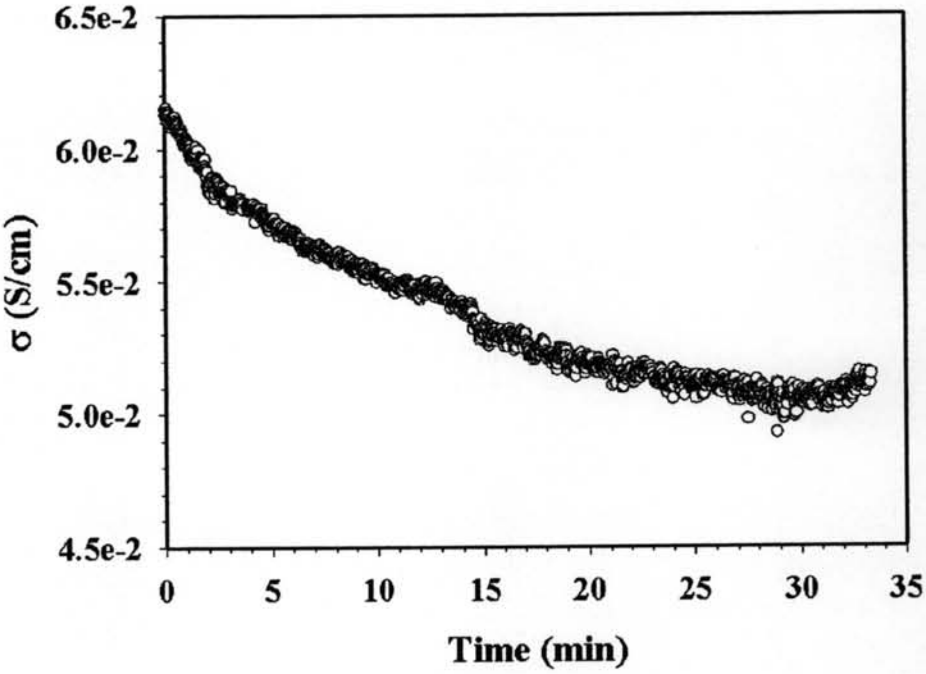

Figure K5 Specific conductivity of 50:1 dPPP when exposed to 0.625%v NH_3.

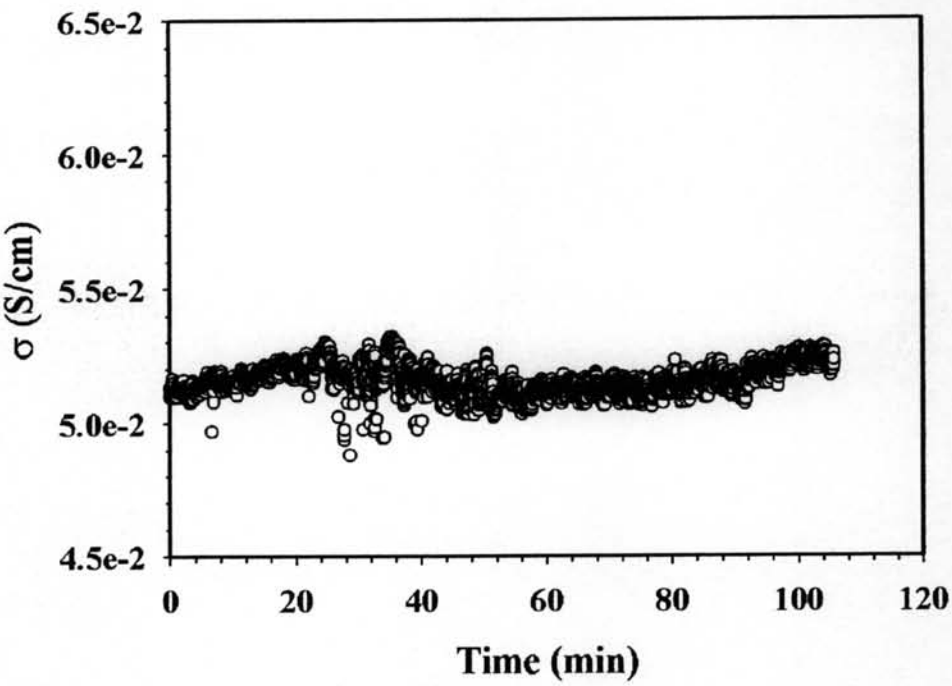

Figure K6 Specific conductivity of 50:1 dPPP after evacuating 0.625%v NH_3 and exposed to N_2.

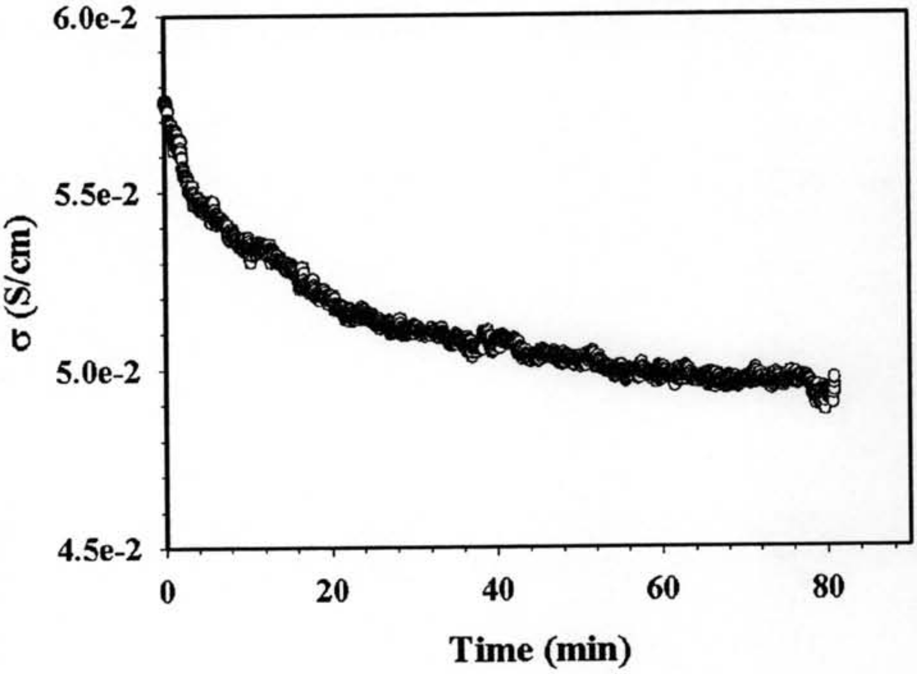

Figure K7 Specific conductivity of 50:1 dPPP when exposed to 1.25%v NH_3.

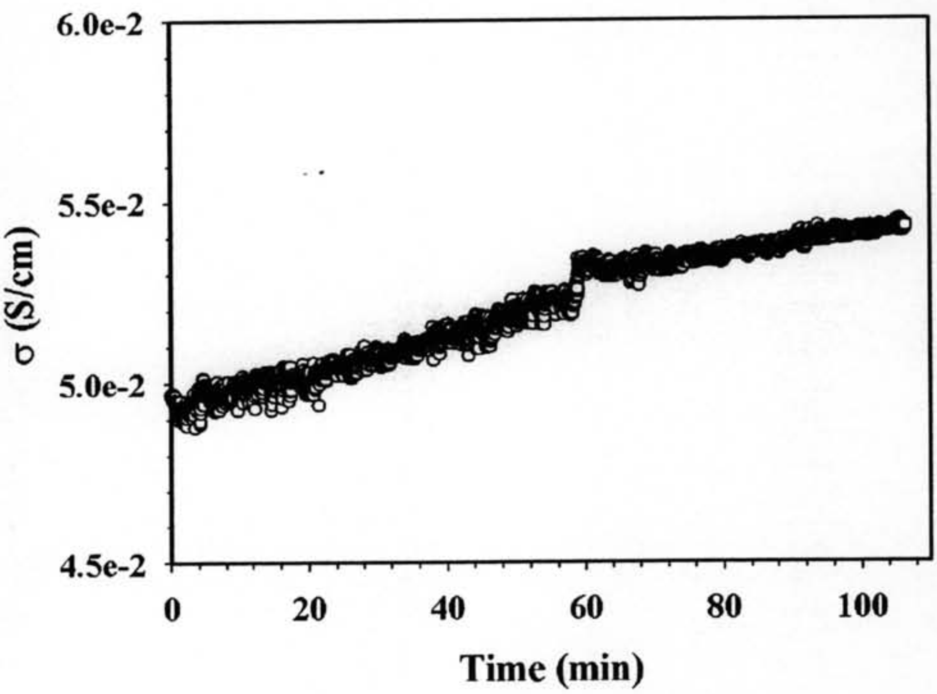

Figure K8 Specific conductivity of 50:1 dPPP after evacuating 1.25%v NH_3 and exposed to N_2.

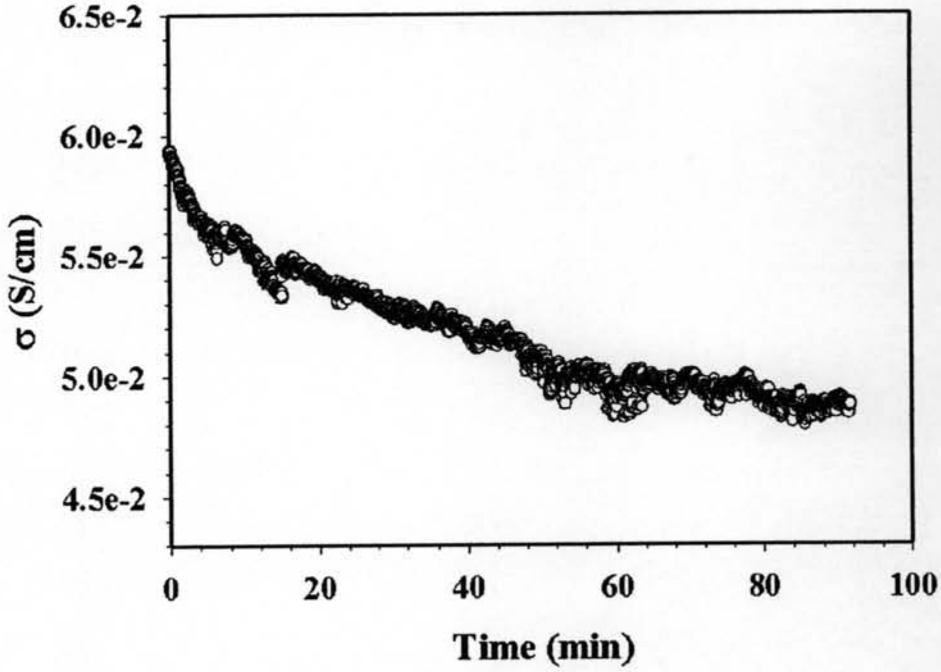

Figure K9 Specific conductivity of 50:1 dPPP when exposed to 2.5%v NH_3.

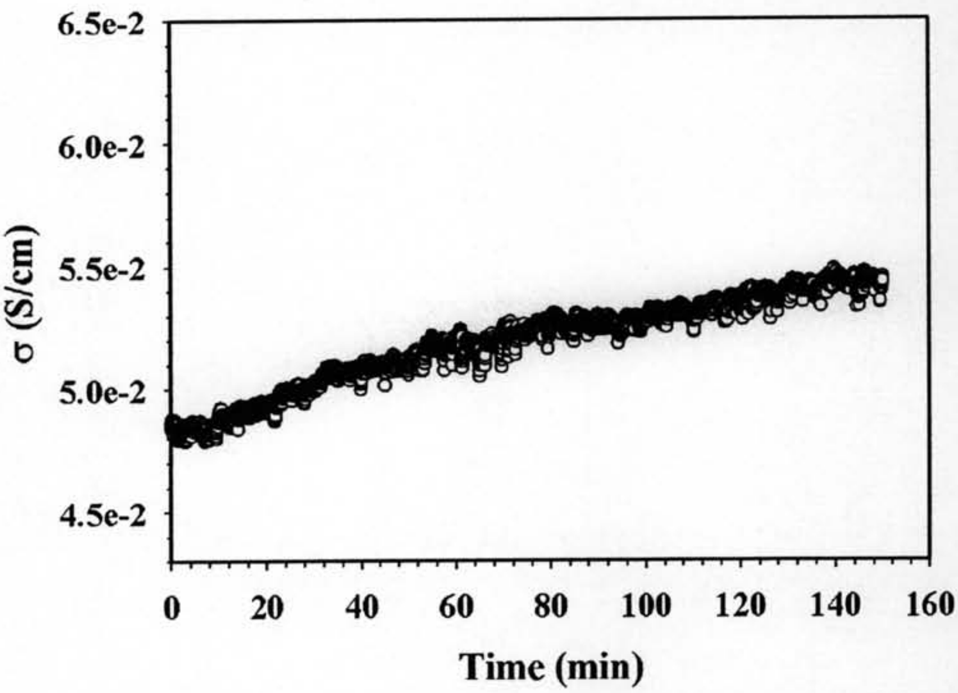

Figure K10 Specific conductivity of 50:1 dPPP after evacuating 2.5%v NH_3 and exposed to N_2.

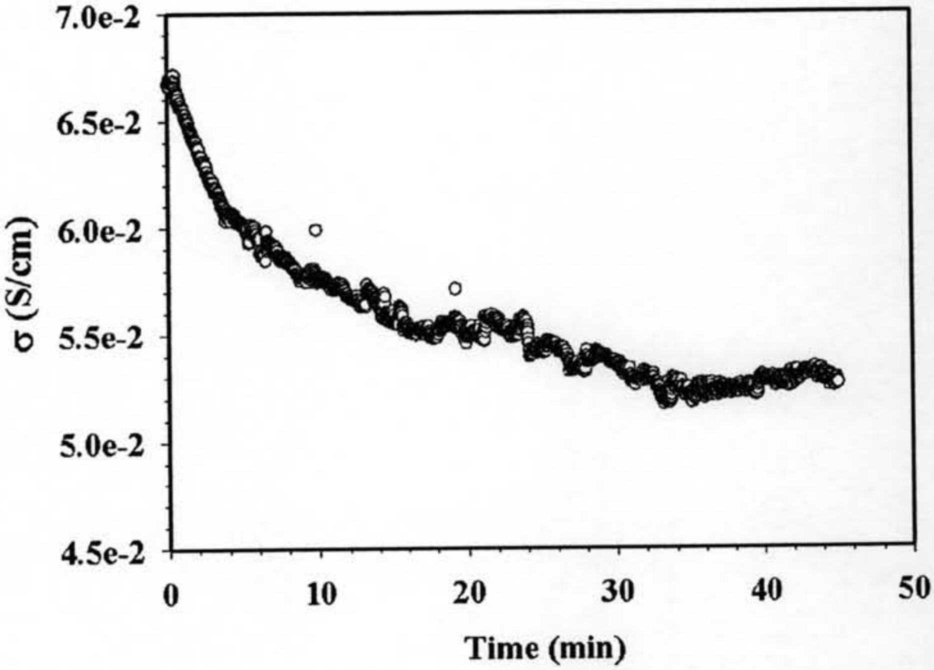

Figure K11 Specific conductivity of 50:1 dPPP when exposed to 5%v NH_3.

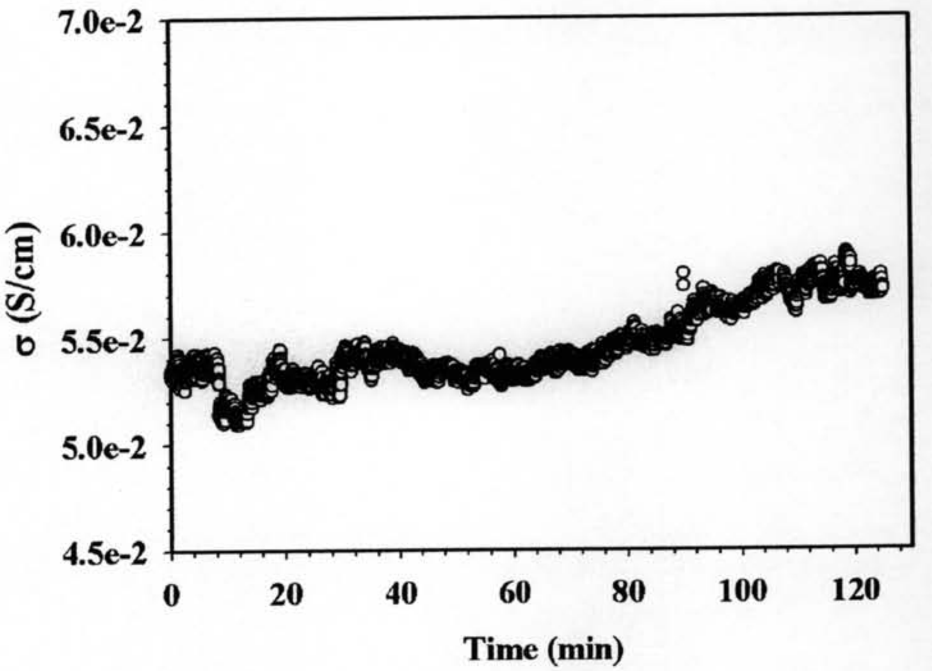

Figure K12 Specific conductivity of 50:1 dPPP after evacuating 5%v NH_3 and exposed to N_2.

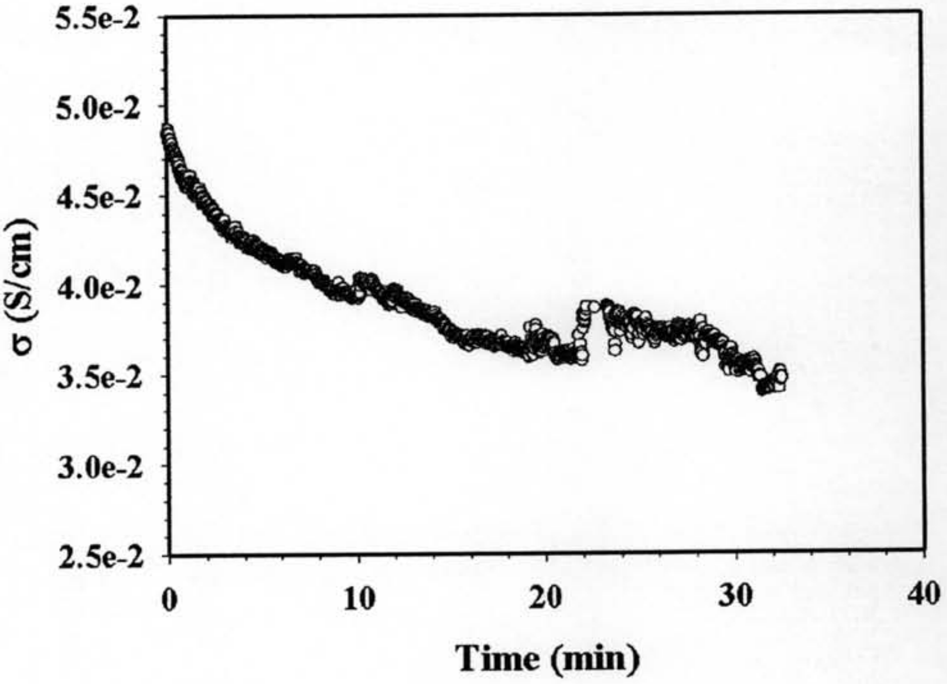

Figure K13 Specific conductivity of 50:1 dPPP when exposed to 10%v NH_3.

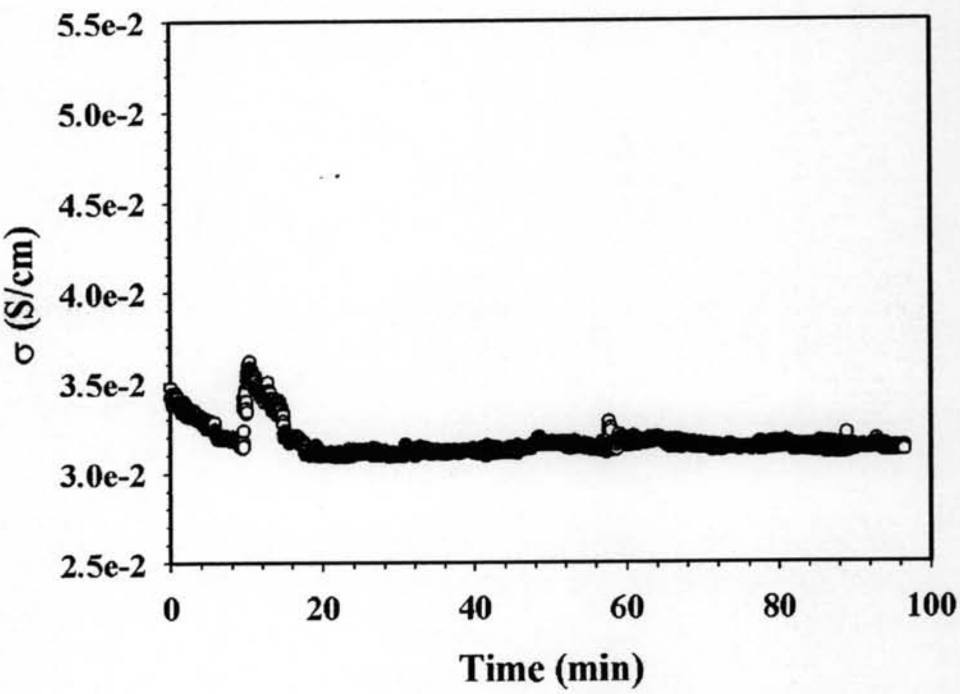

Figure K14 Specific conductivity of 50:1 dPPP after evacuating 10%v NH_3 and exposed to N_2.

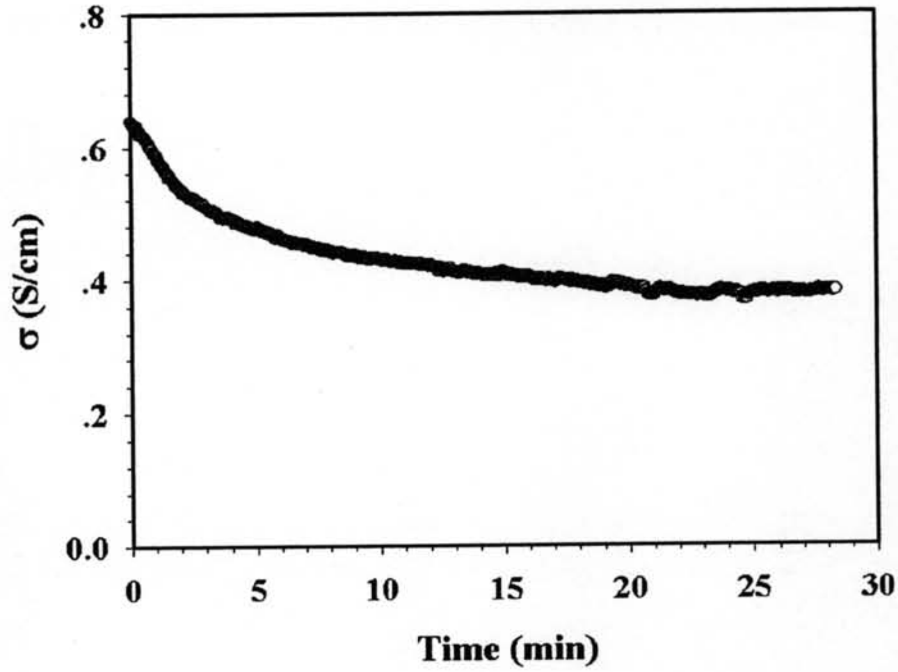

Figure K15 Specific conductivity of dPPP(90)/NaZ23 when exposed to 5%v NH_3.

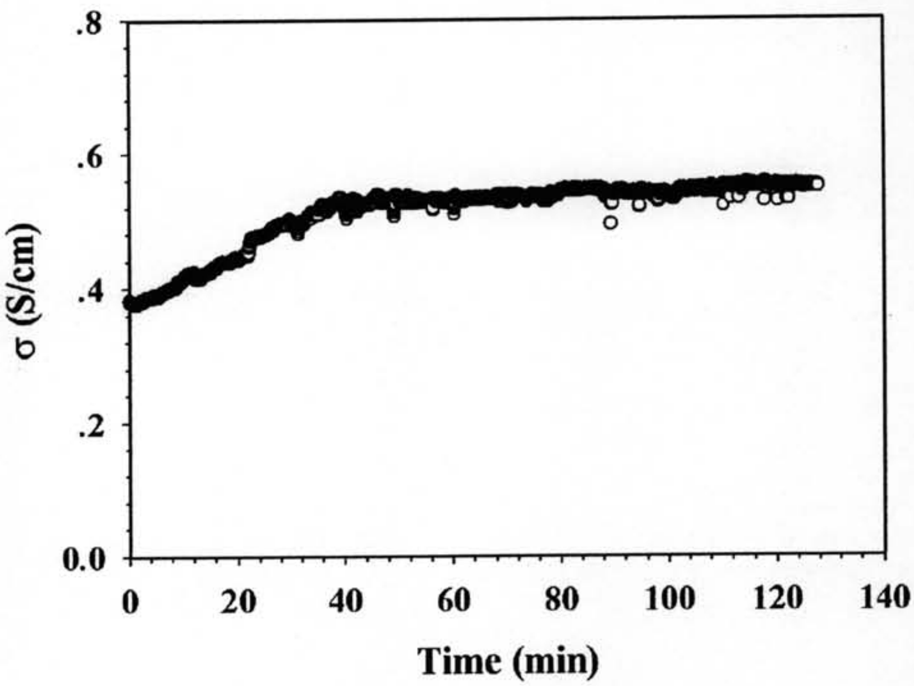

Figure K16 Specific conductivity of dPPP(90)/NaZ23 after evacuating 5%v NH_3 and exposed to N_2.

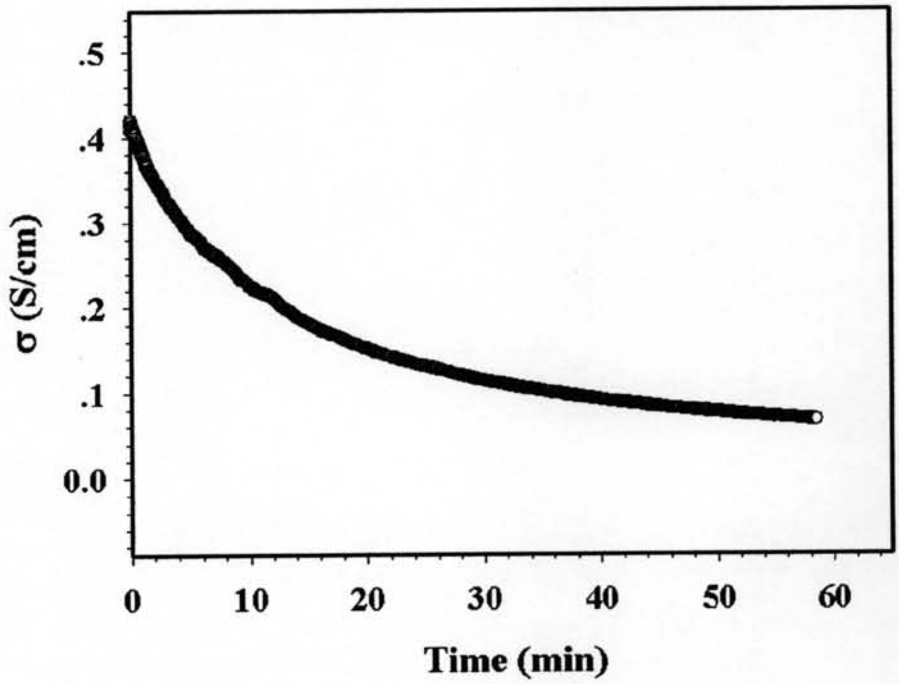

Figure K17 Specific conductivity of dPPP(80)/NaZ23 when exposed to 5%v NH_3.

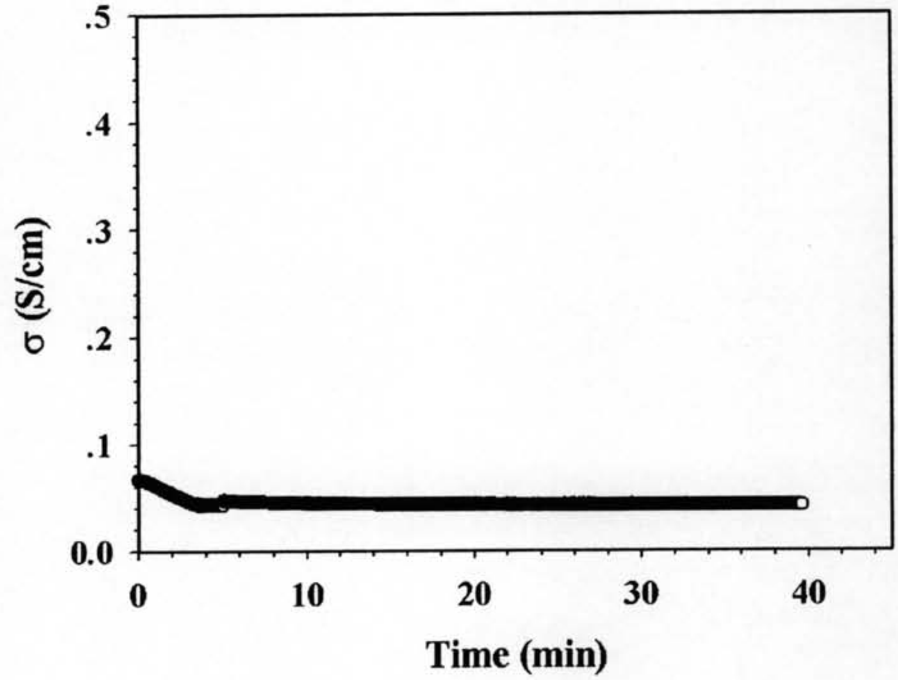

Figure K18 Specific conductivity of dPPP(80)/NaZ23 after evacuating 5%v NH_3 and exposed to N_2.

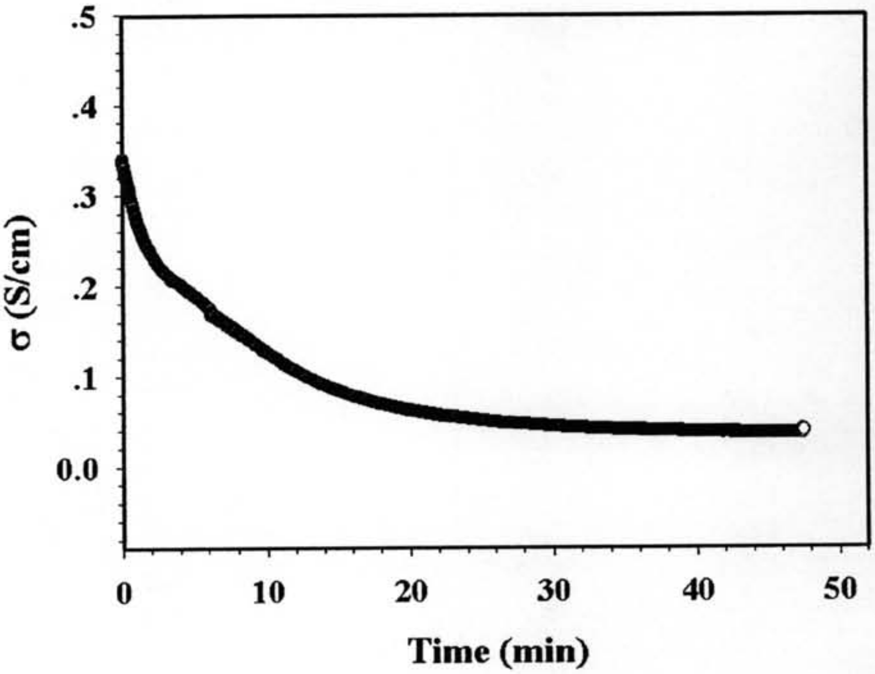

Figure K19 Specific conductivity of dPPP(70)/NaZ23 when exposed to 5%v NH_3.

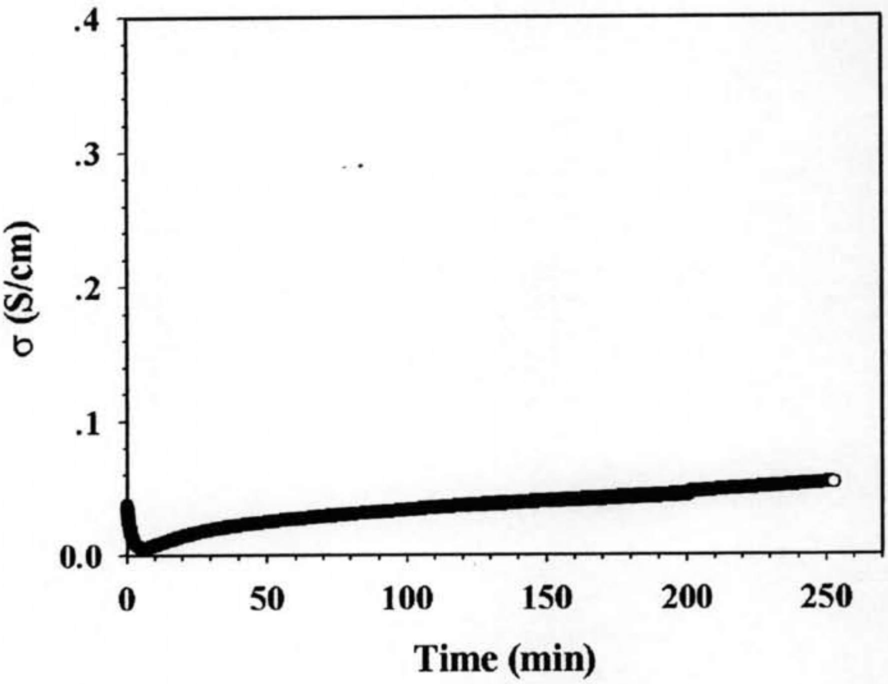

Figure K20 Specific conductivity of dPPP(70)/NaZ23 after evacuating 5%v NH_3 and exposed to N_2.

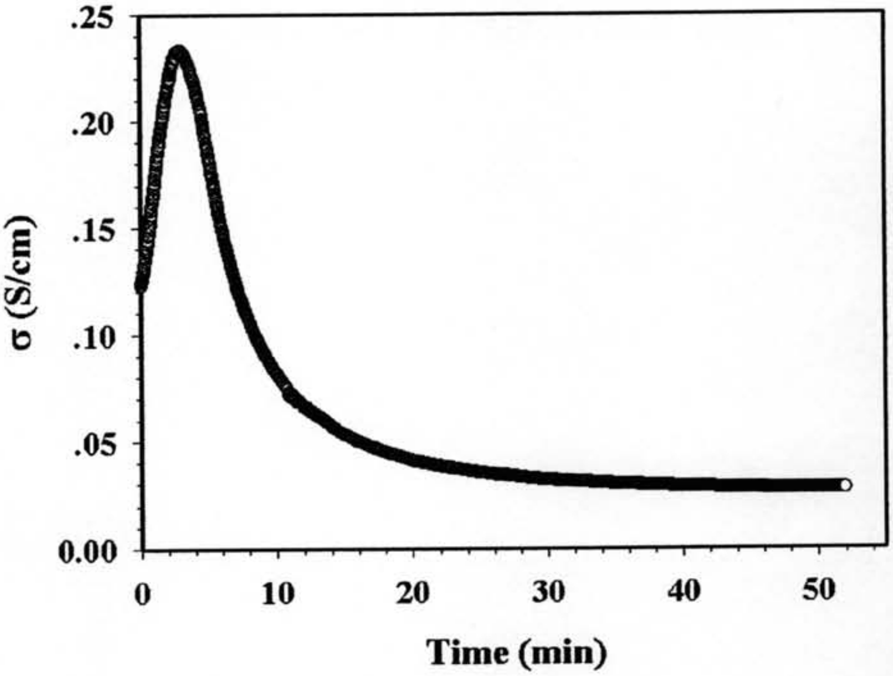

Figure K21 Specific conductivity of dPPP(60)/NaZ23 when exposed to 5%v NH_3.

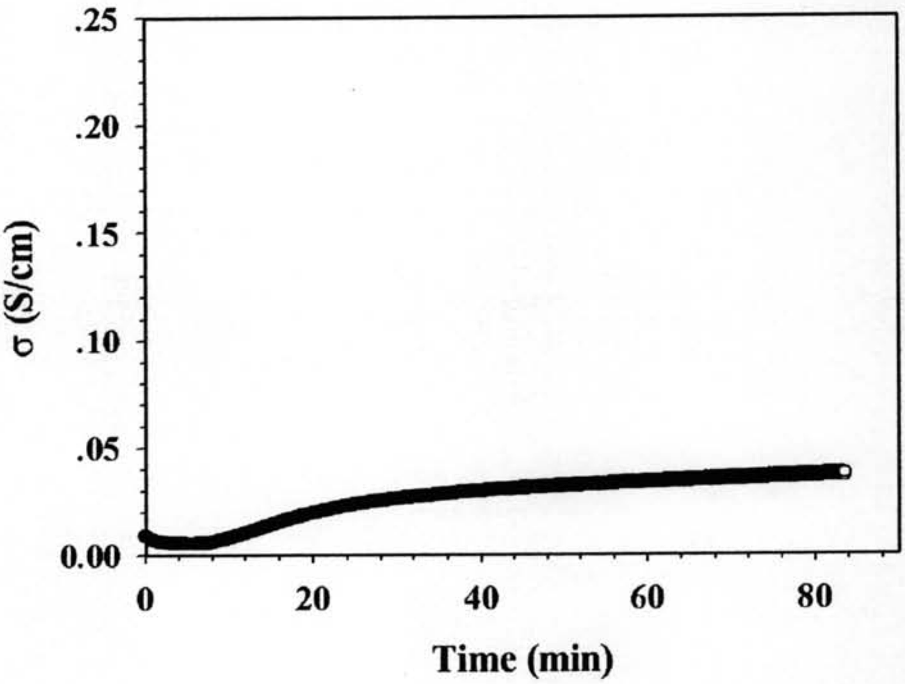

Figure K22 Specific conductivity of dPPP(60)/NaZ23 after evacuating 5%v NH_3 and exposed to N_2.

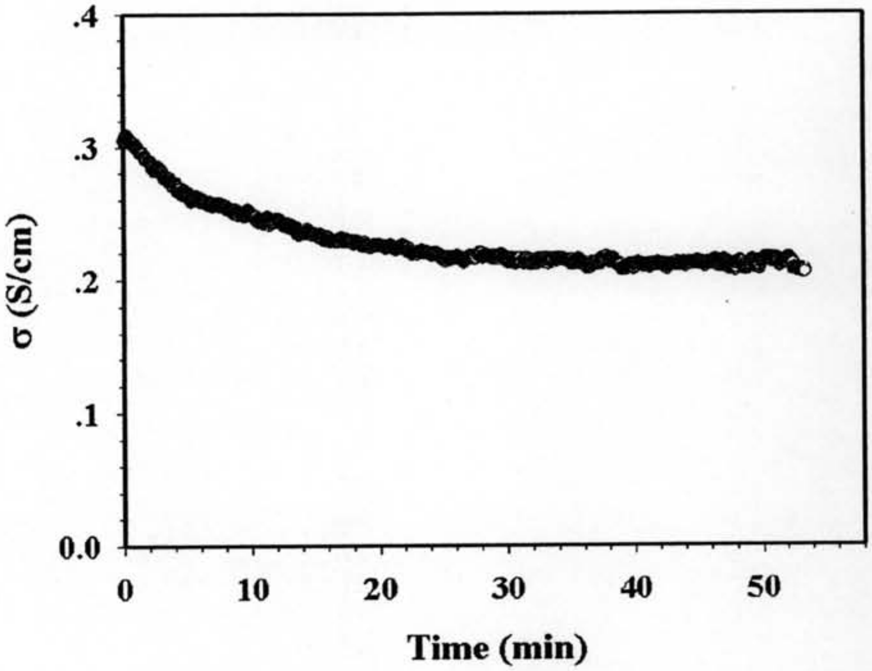

Figure K23 ecific conductivity of dPPP(90)/NaZ23 when exposed to 1.25%v NH_3.

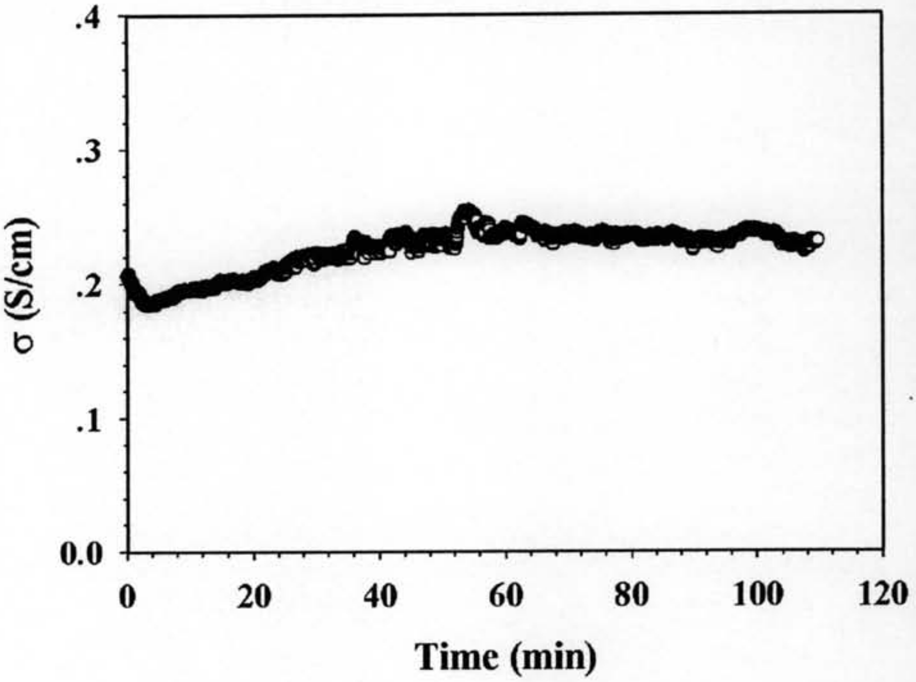

Figure K24 Specific conductivity of dPPP(90)/NaZ23 after evacuating 1.25%v NH_3 and exposed to N_2.

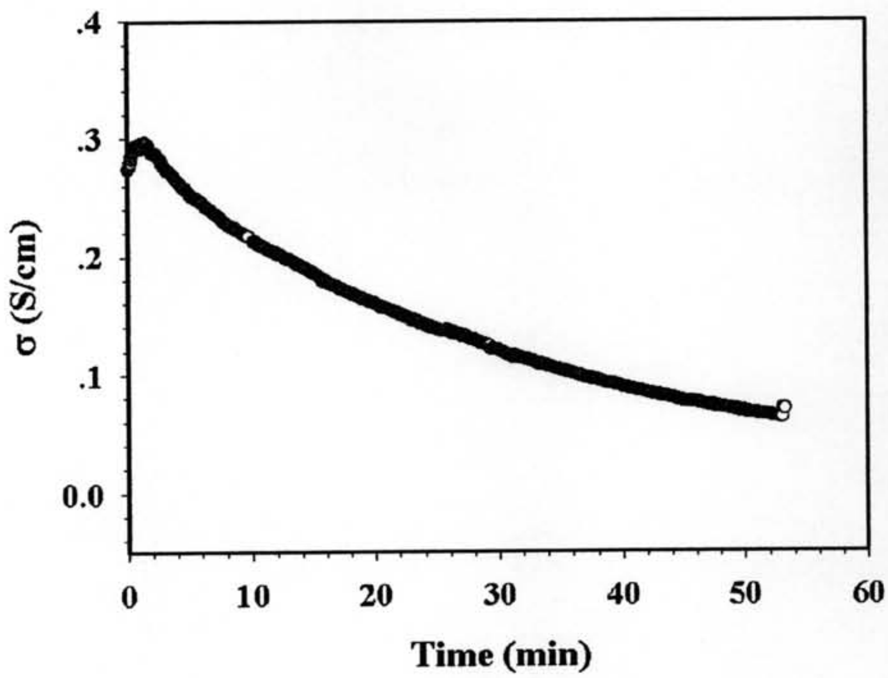

Figure K25 Specific conductivity of dPPP(80)/NaZ23 when exposed to 1.25%v NH_3.

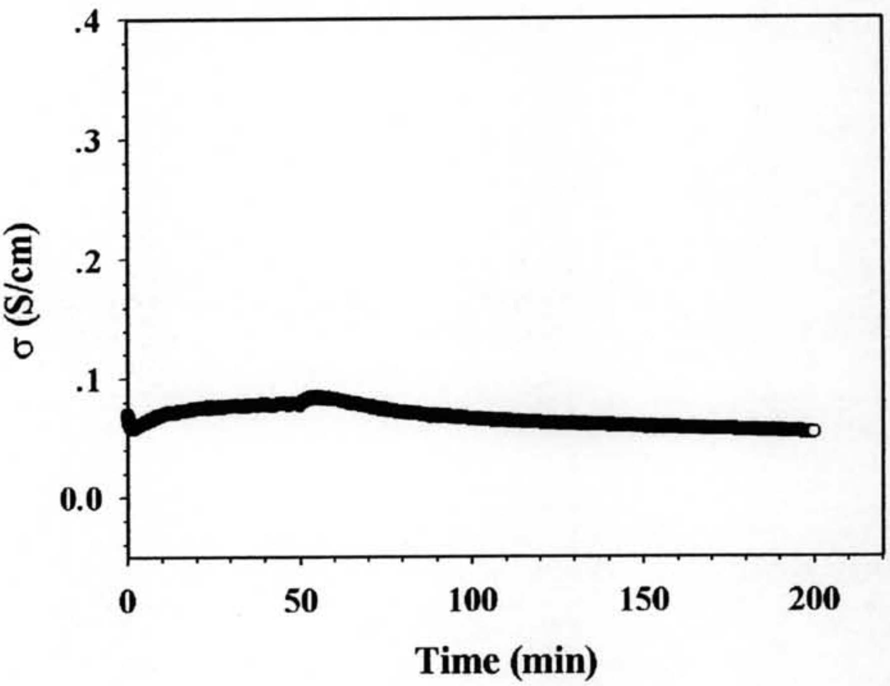

Figure K26 Specific conductivity of dPPP(80)/NaZ23 after evacuating 1.25%v NH_3 and exposed to N_2.

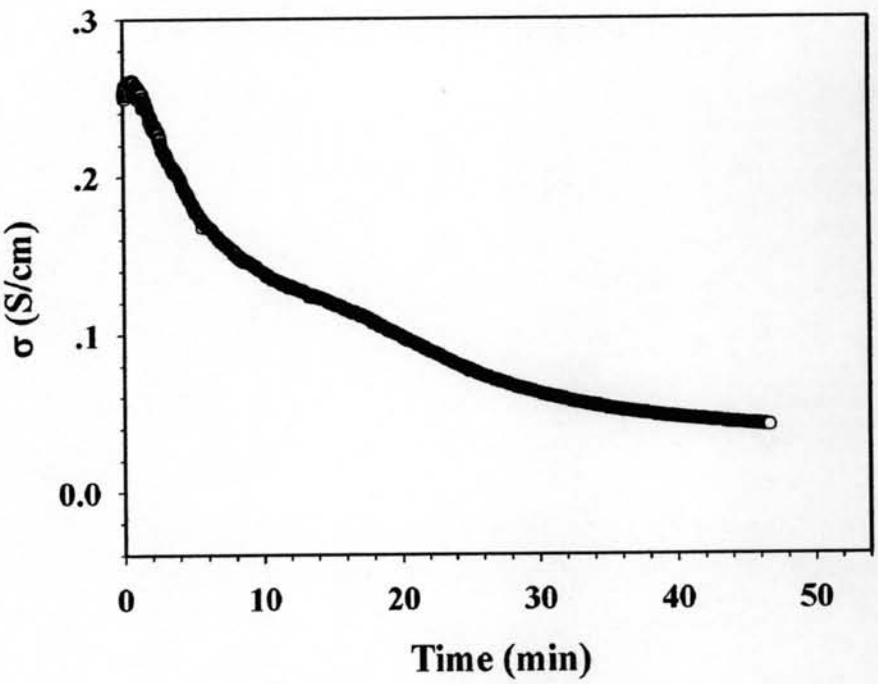

Figure K27 Specific conductivity of dPPP(70)/NaZ23 when exposed to 1.25%v NH_3.

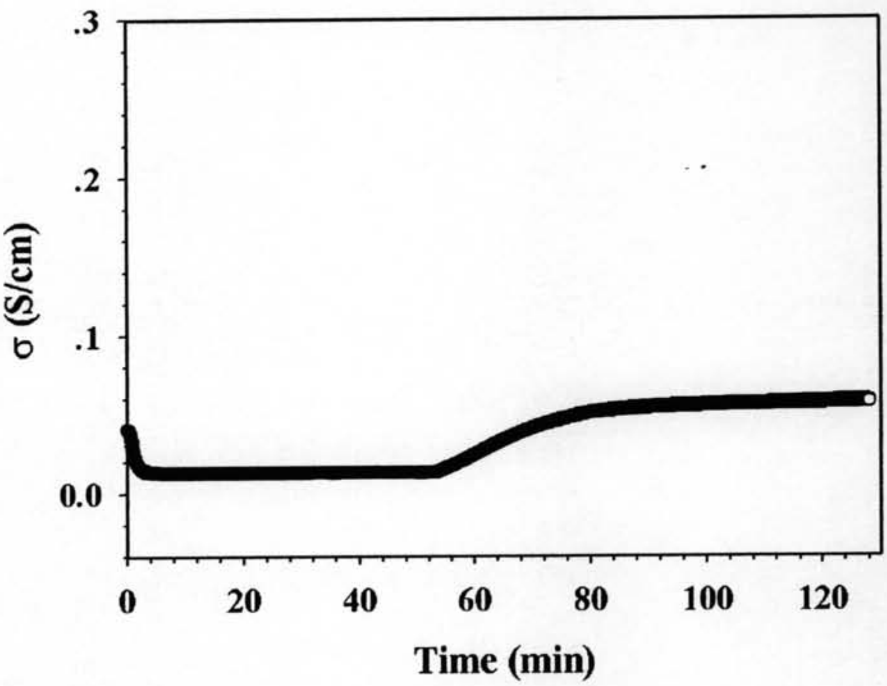

Figure K28 Specific conductivity of dPPP(70)/NaZ23 after evacuating 1.25%v NH_3 and exposed to N_2.

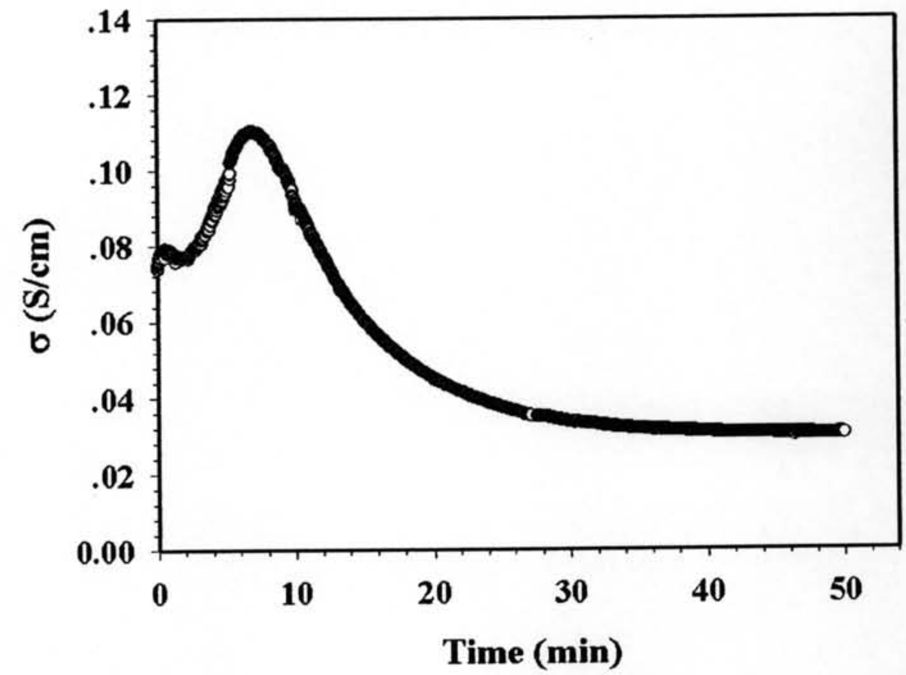

Figure K29 Specific conductivity of dPPP(60)/NaZ23 when exposed to 1.25%v NH_3.

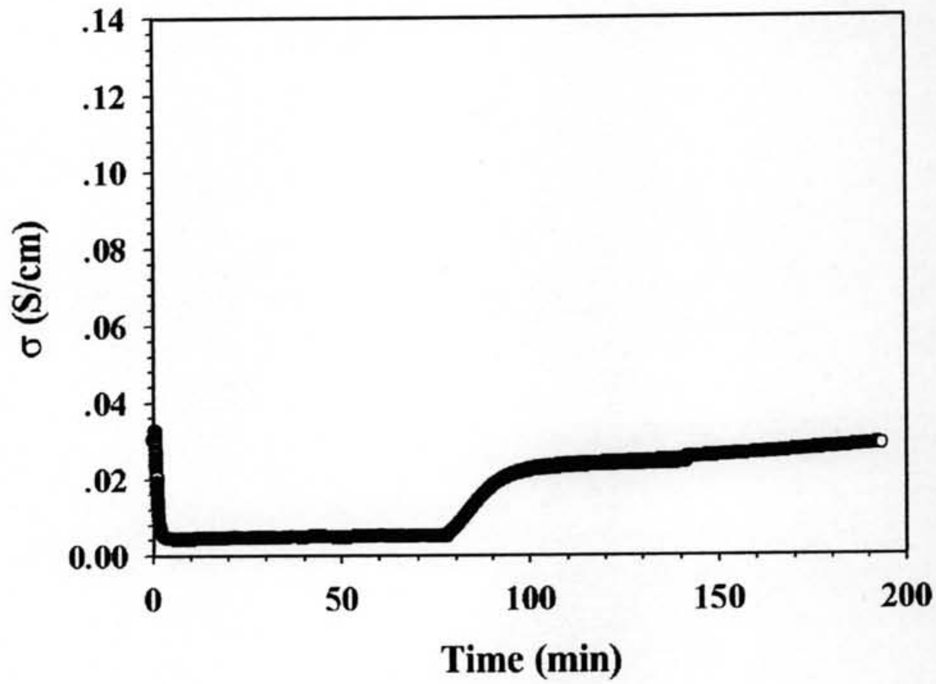

Figure K30 Specific conductivity of dPPP(60)/NaZ23 after evacuating 1.25%v NH_3 and exposed to N_2.

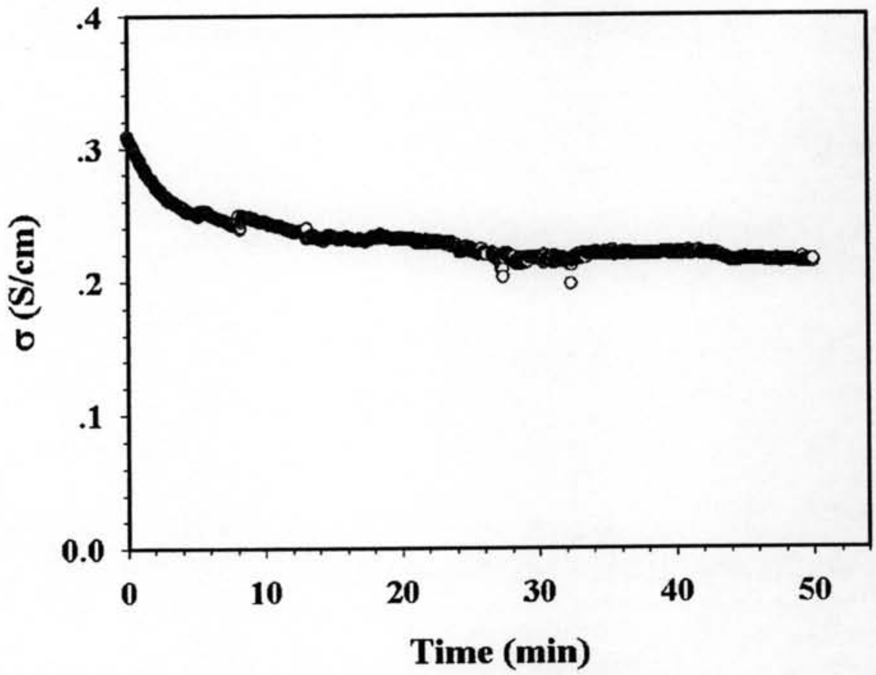

Figure K31 Specific conductivity of dPPP(90)/NaZ23 when exposed to 0.625%v NH_3.

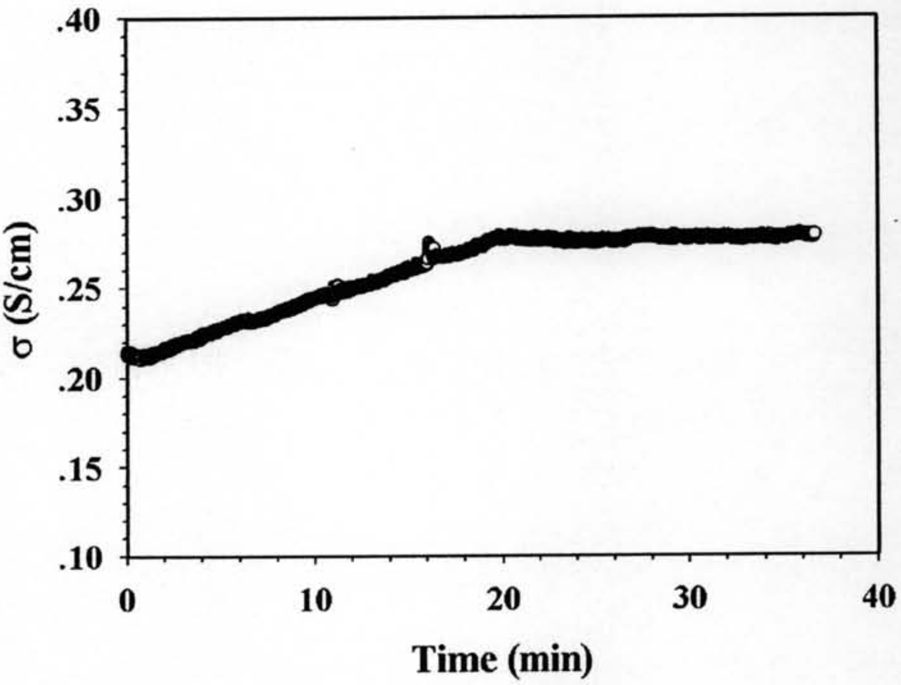

Figure K32 Specific conductivity of dPPP(90)/NaZ23 after evacuating 0.625%v NH_3 and exposed to N_2.

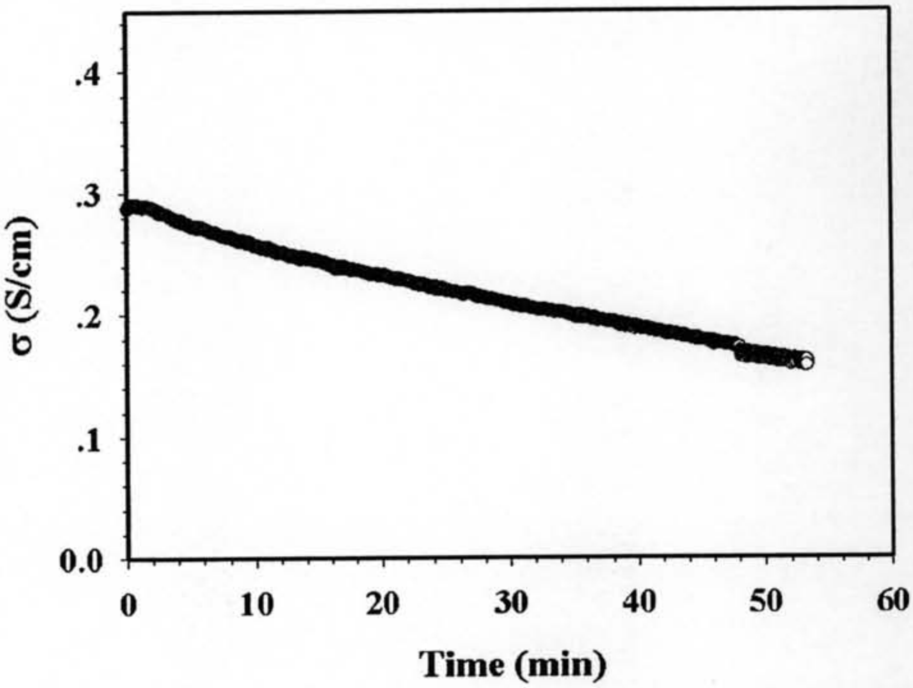

Figure K33 Specific conductivity of dPPP(80)/NaZ23 when exposed to 0.625%v NH_3.

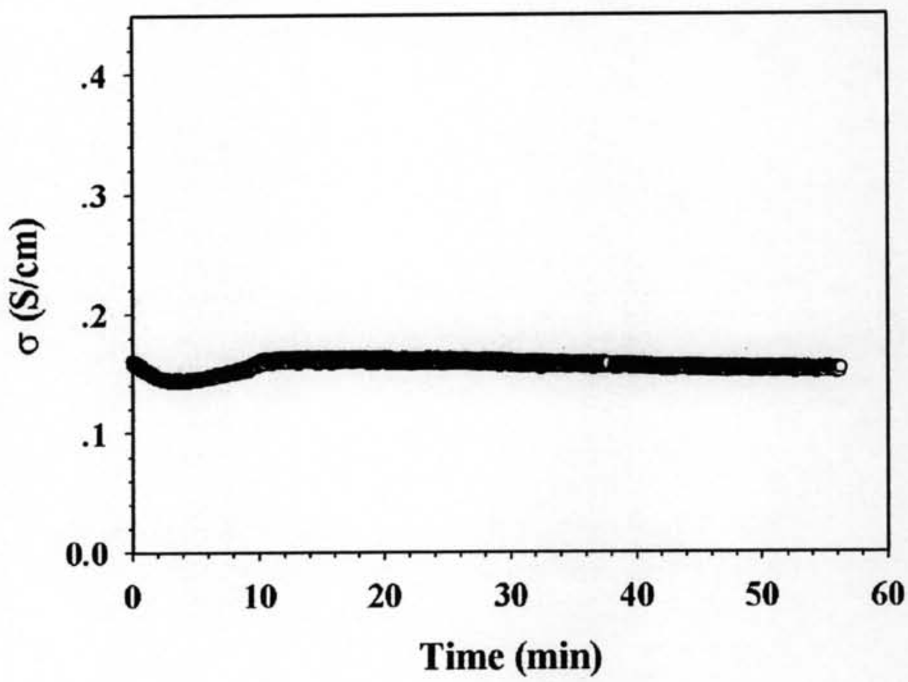

Figure K34 Specific conductivity of dPPP(80)/NaZ23 after evacuating 0.625%v NH_3 and exposed to N_2.

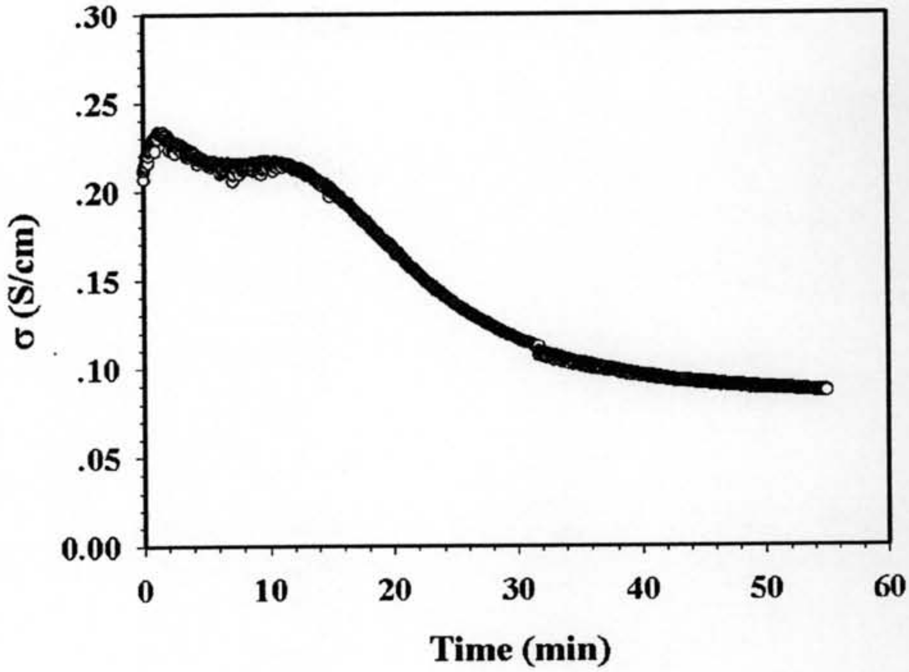

Figure K35 Specific conductivity of dPPP(70)/NaZ23 when exposed to 0.625%v NH_3.

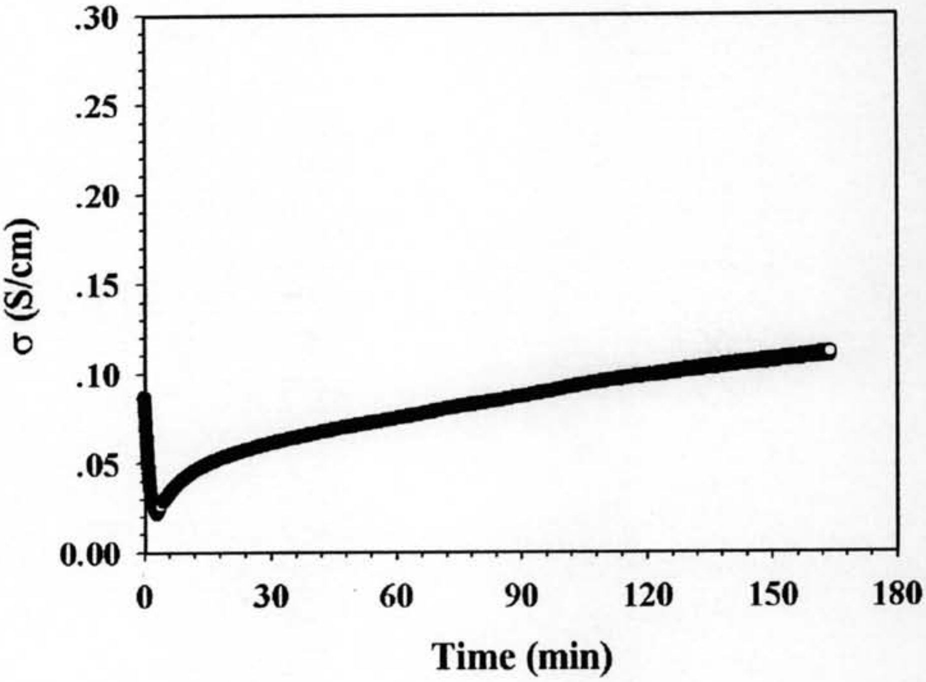

Figure K36 Specific conductivity of dPPP(70)/NaZ23 after evacuating 0.625%v NH_3 and exposed to N_2.

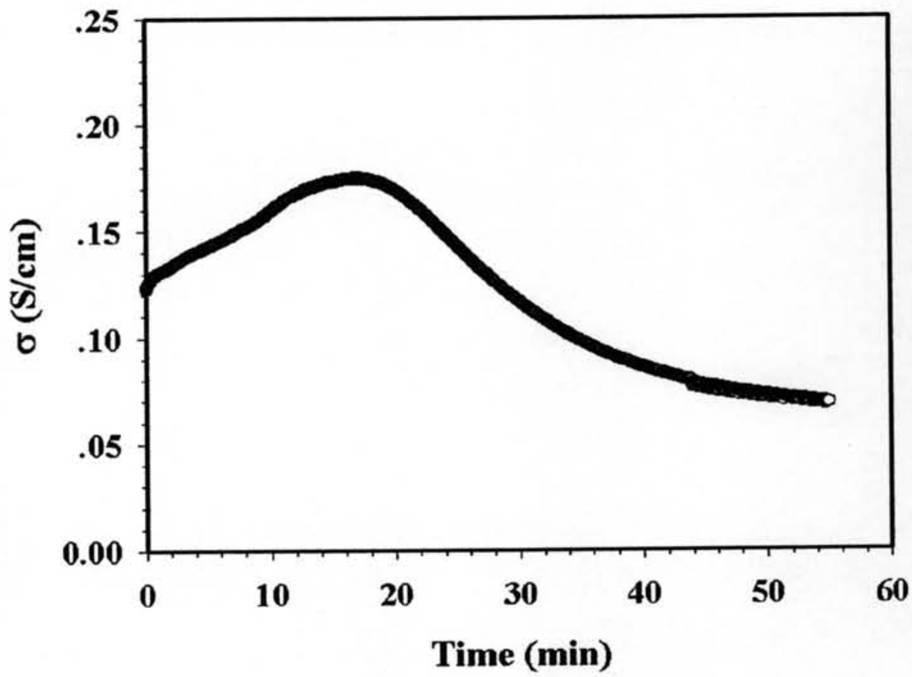

Figure K37 Specific conductivity of dPPP(60)/NaZ23 when exposed to 0.625%v NH_3.

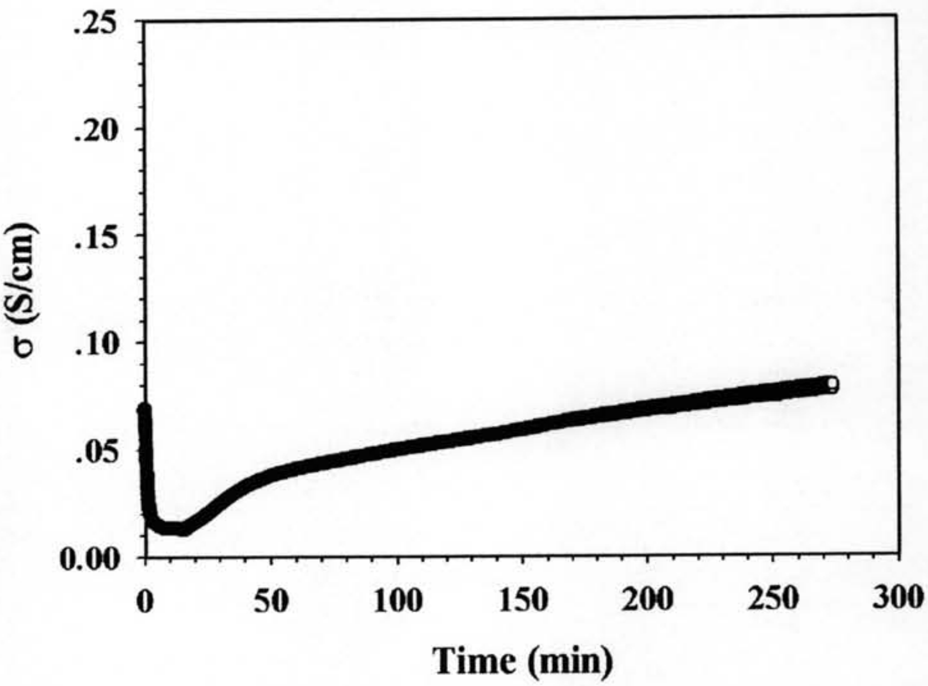

Figure K38 Specific conductivity of dPPP(60)/NaZ23 after evacuating 0.625%v NH_3 and exposed to N_2.

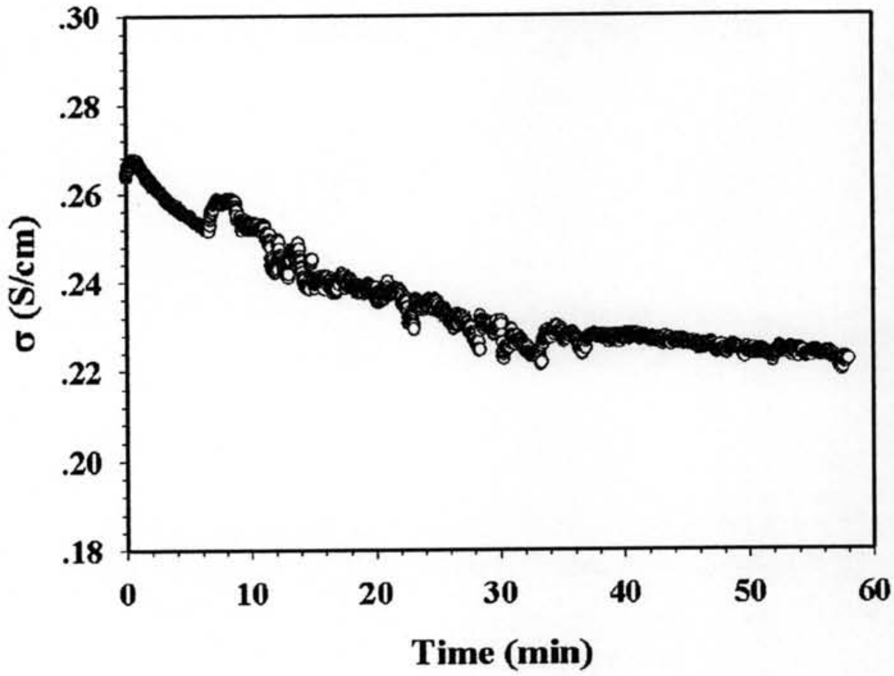

Figure K39 Specific conductivity of dPPP(90)/KZ23 when exposed to 0.625%v NH_3.

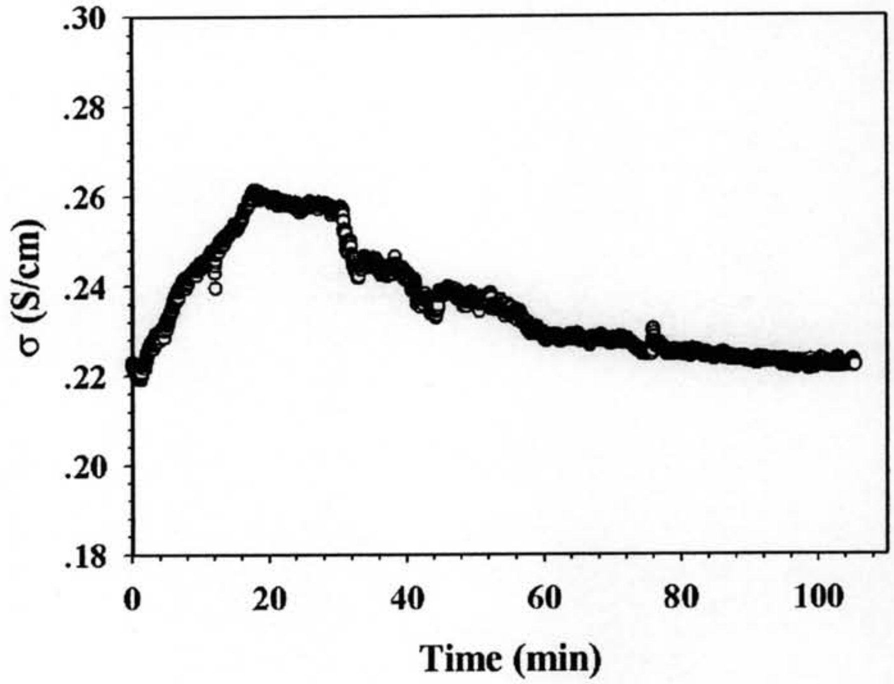

Figure K40 Specific conductivity of dPPP(90)/KZ23 after evacuating 0.625%v NH_3 and exposed to N_2.

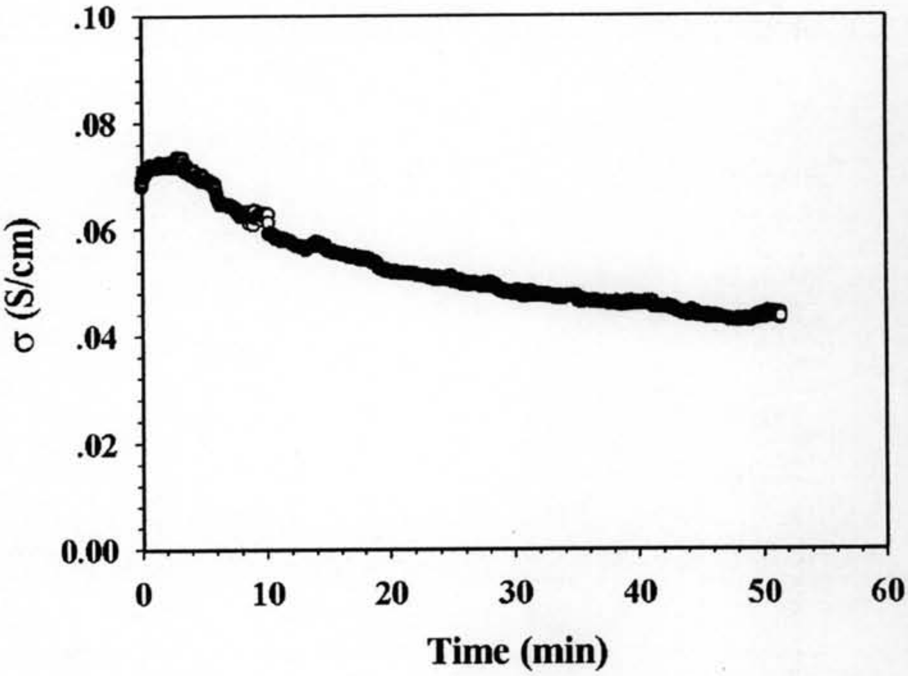

Figure K41 Specific conductivity of dPPP(90)/NH_4Z23 when exposed to 0.625%v NH_3.

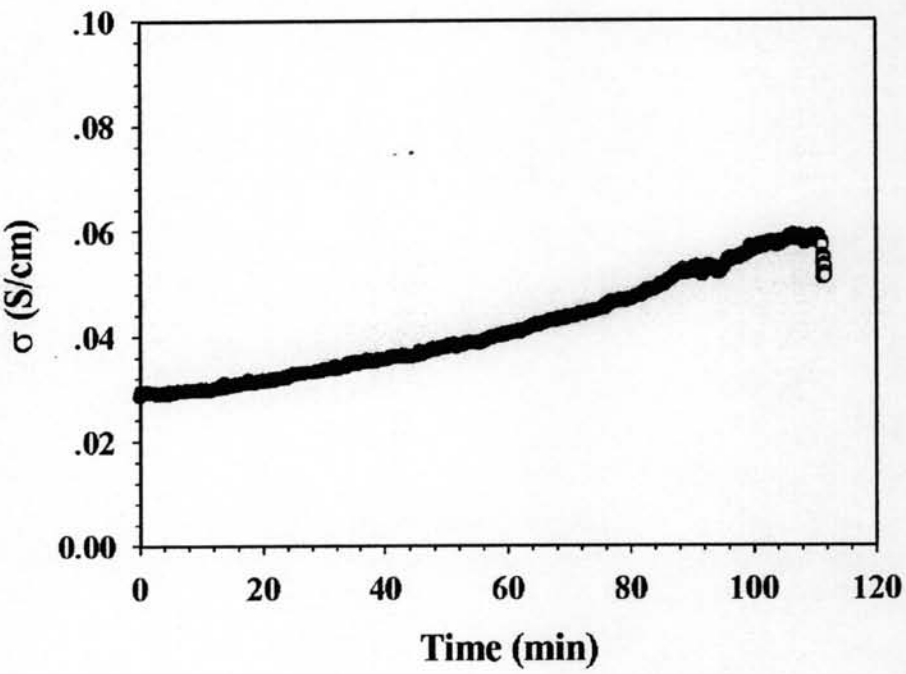

Figure K42 Specific conductivity of dPPP(90)/NH_4Z23 after evacuating 0.625%v NH_3 and exposed to N_2.

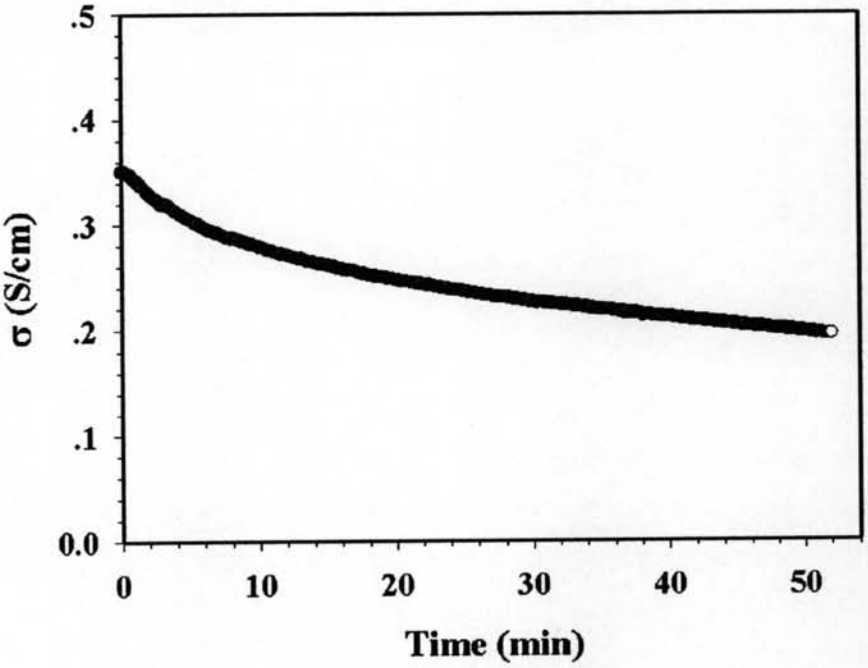

Figure K43 Specific conductivity of dPPP(90)/HZ23 when exposed to 0.625%v NH_3.

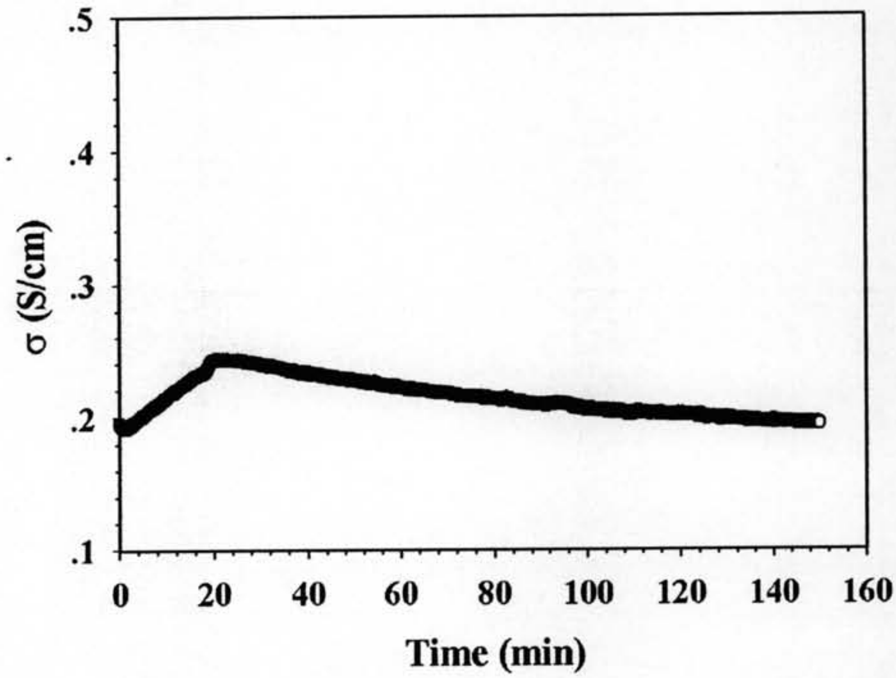

Figure K44 Specific conductivity of dPPP(90)/HZ23 after evacuating 0.625%v NH_3 and exposed to N_2.

Table K1 Specific conductivity and sensitivity of 50:1dPPP and its composites when exposed to air, N_2 and NH_3 with various concentrations under chamber temperature (T_c) of 28±1 °C, at 1 atm, t_i = the time that σ_{NH_3} reaches equilibrium, t_r = the time that σ reaches equilibrium after evacuate NH_3, V = applied voltage, K = correction factor (2.19 × 10^{-5})

No.	Samples	Thickness (cm)	V (V)	[NH_3] (% v.)	t_i (min)	t_r (min)	I (A)				σ (S/cm)				Response	Sensitivity
							Air	N_2 initial	NH_3	N_2 final	Air	N_2 initial	NH_3	N_2 final		
1	50:1dPPP	0.04127	25	0.15625	106.68	228.54	(7.38± 0.12)E-7	(6.78± 0.04)E-7	(6.09± 0.02)E-7	(6.71± 0.03)E-7	(3.26± 0.05)E-2	(2.99± 0.02)E-2	(2.69± 0.01)E-2	(2.96± 0.01)E-2	(-3.04± 0.24)E-3	(-9.81± 0.71)E-2
2	50:1dPPP	0.02736	25	0.3125	65.84	145.04	(5.18± 0.07)E-7	(4.16± 0.03)E-7	(3.62± 0.06)E-7	(4.06± 0.02)E-7	(3.45± 0.05)E-2	(2.78± 0.02)E-2	(2.42± 0.04)E-2	(2.68± 0.02)E-2	(-3.61± 0.52)E-3	(-1.15± 0.07)E-1
3	50:1dPPP	0.02054	20	0.625	33.34	105.00	(9.86± 0.85)E-7	(5.39± 0.01)E-7	(4.6± 0.02)E-7	(4.71± 0.21)E-7	(1.09± 0.09)E-1	5.98± 0.01)E-2	(5.10± 0.03)E-2	(5.23± 0.02)E-2	(-8.85± 0.33)E-3	(-1.43± 0.02)E-1
4	50:1dPPP	0.02538	20	0.625	80.84	62.99	(4.29± 0.17)E-7	(4.17± 0.05)E-7	(3.62± 0.08)E-7	3.99± 0.04)E-7	(3.85± 0.15)E-2	(3.75± 0.05)E-2	(3.25± 0.07)E-2	(3.58± 0.03)E-2	(-4.98± 0.97)E-3	(-1.14± 0.15)E-1
5	50:1dPPP	0.02512	20	1.25	80.84	132.24	(1.17± 0.09)E-6	(6.28± 0.01)E-7	(5.43± 0.02)E-7	(5.99± 0.02)E-7	(1.06± 0.08)E-1	(5.70± 0.01)E-2	(4.93± 0.02)E-2	(5.43± 0.02)E-2	(-7.72± 0.22)E-3	(-1.33± 0.02)E-1
6	50:1dPPP	0.02252	20	1.25	107.5	68.1	(4.97± 0.10)E-7	(3.73± 0.03)E-7	(3.05± 0.03)E-7	(3.13± 0.04)E-7	(5.03± 0.10)E-2	(3.78± 0.03)E-2	(3.09± 0.03)E-2	(3.17± 0.04)E-2	(-6.87± 0.49)E-3	(-1.74± 0.09)E-1
7	50:1dPPP	0.02049	25	1.25	83.34	111.77	(3.50± 0.22)E-7	(4.73± 0.05)E-7	(3.96± 0.1)E-7	(4.59± 0.15)E-7	(3.11± 0.19)E-2	(4.21± 0.04)E-2	(3.52± 0.10)E-2	(4.08± 0.10)E-2	(-6.87± 1.24)E-3	(-1.40± 0.12)E-1
8	50:1dPPP	0.02296	20	2.5	91.67	150	(6.83± 0.29)E-7	(5.98± 0.03)E-7	(4.92± 0.01)E-7	(5.47± 0.01)E-7	(6.77± 0.29)E-2	(5.93± 0.03)E-2	(4.88± 0.01)E-2	(5.43± 0.01)E-2	(-1.05± 0.04)E-2	(-1.75± 0.07)E-1
9	50:1dPPP	0.02145	25	2.5	75.01	130.31	(4.93± 0.30)E-7	(4.53± 0.04)E-7	(3.69± 0.04)E-7	(4.14± 0.02)E-7	(4.19± 0.25)E-2	(3.85± 0.03)E-2	(3.14± 0.04)E-2	(3.52± 0.01)E-2	(-7.17± 0.55)E-3	(-1.76± 0.09)E-1
10	50:1dPPP	0.02256	20	5	75.84	86.67	(9.88± 0.75)E-7	(3.75± 0.04)E-7	(2.96± 0.08)E-7	(3.20± 0.02)E-7	(9.98± 0.76)E-2	(3.79± 0.04)E-2	(2.99± 0.09)E-2	(3.23± 0.02)E-2	(-8.04± 0.11)E-3	(-2.12± 0.12)E-1
11	50:1dPPP	0,0204	20	5	45	125	(9.71± 0.64)E-7	(5.73± 0.01)E-7	(4.71± 0.03)E-7	(5.15± 0.04)E-7	(1.08± 0.07)E-1	(6.40± 0.01)E-2	(5.26± 0.03)E-2	(5.75± 0.04)E-2	(-1.14± 0.04)E-2	(-1.77± 0.03)E-1
12	50:1dPPP	0.02097	25	10	32.51	96.49	(5.95± 0.08)E-7	(5.52± 0.05)E-7	(4.05± 0.09)E-7	(3.60± 0.01)E-7	(5.17± 0.07)E-2	(4.80± 0.04)E-2	(3.52± 0.07)E-2	(3.13± 0.01)E-2	(-1.28± 0.1)E-2	(-2.51± 0.10)E-1

No.	Samples	Thickness (cm)	V (V)	$[NH_3]$ (% v.)	t_i (min)	t_r (min)	I (A)				σ (S/cm)				Response	Sensitivity
							Air	N_2 initial	NH_3	N_2 final	Air	N_2 initial	NH_3	N_2 final		
13	50:1dPPP(90)/NaZ23	0.02084	12	5	28.34	127.7	(1.05± 0.02)E-5	(3.09± 0.01)E-6	(2.07± 0.01)E-6	(3.02± 0.00)E-6	(1.92± 0.04)E0	(5.63± 0.01)E-1	(3.78± 0.07)E-1	(5.50± 0.00)E-1	(-1.85± 0.03)E-1	(-3.24± 0.03)E-1
14	50:1dPPP(90)/NaZ23	0.02977	12	5	53.34	148.04	(4.27± 0.18)E-6	(2.01± 0.03)E-6	(1.07± 0.01)E-6	(1.16± 0.00)E-6	(5.45± 0.23)E-1	(2.57± 0.04)E-1	(1.37± 0.00)E-1	(1.48± 0.00)E-1	(-1.20± 0.05)E-1	(-4.64± 0.21)E-1
15	50:1dPPP(80)/NaZ23	0.021	15	5	58.53	39.61	(5.74± 0.19)E-6	(2.32± 0.12)E-6	(4.79± 0.10)E-7	(2.92± 0.01)E-7	(8.30± 0.27)E-1	(3.35± 0.17)E-1	(6.93± 0.15)E-2	(4.23± 0.83)E-2	(-2.66± 0.20)E-1	(-7.91± 0.75)E-1
16	50:1dPPP(70)/NaZ23	0.02114	25	5	47.51	252.79	(1.41± 0.02)E-4	(3.71± 0.01)E-6	(4.34± 0.13)E-7	(6.19± 0.01)E-7	(1.21± 0.02)E+1	(3.20± 0.01)E-1	(3.74± 0.11)E-2	(5.34± 0.01)E-2	(-2.83± 0.02)E-1	(-8.80± 0.03)E-1
17	50:1dPPP(60)/NaZ23	0.02452	50	5	54.17	83.57	(9.53± 4.34)E-6	(2.73± 0.01)E-6	(7.54± 0.08)E-7	(1.00± 0.01)E-6	(3.54± 1.61)E-1	(1.01± 0.01)E-1	(2.80± 0.03)E-2	(4.35± 0.04)E-2	(-7.34± 0.06)E-2	(-7.21± 0.06)E-1
18	50:1dPPP(90)/NaZ23	0.01383	10	1.25	53.34	109.8	(1.70± 0.02)E-5	(9.19± 0.05)E-7	(6.41± 0.09)E-7	(6.92± 0.07)E-7	(5.59± 0.07)E0	(3.03± 0.02)E-1	(2.11± 0.03)E-1	(2.28± 0.02)E-1	(-9.16± 0.39)E-2	(-2.93± 0.06)E-1
20	50:1dPPP(80)/NaZ23	0.01969	30	1.25	53.34	137.24	(2.26± 0.32)E-5	(2.81± 0.03)E-6	(1.32± 0.01)E-6	(8.15± 0.02)E-7	(1.74± 0.25)E0	(2.17± 0.02)E-1	(1.02± 0.01)E-1	(6.29± 0.01)E-2	(-1.15± 0.03)E-1	(-5.26± 0.14)E-1
21	50:1dPPP(70)/NaZ23	0.01813	40	1.25	50.84	128.16	(2.40± 0.11)E-5	(3.42± 0.02)E-6	(6.80± 0.22)E-7	(9.19± 0.06)E-7	(1.51± 0.07)E0	(2.15± 0.01)E-1	(4.27± 0.14)E-2	(5.77± 0.04)E-2	(-1.72± 0.02)E-1	(-7.95± 0.09)E-1
22	50:1dPPP(60)/NaZ23	0.01929	50	1.25	50	193.48	(6.19± 0.47)E-6	(1.45± 0.01)E-6	(6.44± 0.15)E-7	(6.09± 0.01)E-7	(2.93± 0.45)E-1	(6.84± 0.02)E-2	(3.04± 0.01)E-2	(2.65± 0.00)E-2	(-3.8± 0.03)E-1	(-5.55± 0.04)E-1
23	50:1dPPP(90)/NaZ23	0.01504	8	0.625	50	36.67	(1.68± 0.09)E-6	(7.31± 0.02)E-7	(5.68± 0.02)E-7	(7.34± 0.02)E-7	(6.37± 0.32)E-1	(2.77± 0.01)E-1	(2.15± 0.01)E-1	(2.8± 0.06)E-1	(-6.20± 0.11)E-2	(-2.21± 0.02)E-1
24	50:1dPPP(80)/NaZ23	0.01778	30	0.625	53.34	56.27	(8.60± 0.05)E-6	(3.09± 0.02)E-6	(1.89± 0.02)E-6	(1.80± 0.01)E-6	(7.35± 0.04)E-1	(2.64± 0.01)E-1	(1.61± 0.02)E-1	(1.53± 0.01)E-1	(-1.03± 0.02)E-1	(-3.84± 0.05)E-1
25	50:1dPPP(70)/NaZ23	0.01639	50	0.625	55	164.04	(1.57± 0.10)E-5	(3.25± 0.03)E-6	(1.57± 0.01)E-6	(1.99± 0.01)E-6	(8.75± 0.56)E-2	(1.81± 0.02)E-1	(8.76± 0.04)E-1	(1.11± 0.07)E-1	(-9.33± 0.20)E-2	(-5.14± 0.12)E-1
26	50:1dPPP(60)/NaZ23	0.02963	70	0.625	55	273.94	(1.33± 0.04)E-5	(2.76± 0.54)E-6	(1.79± 0.04)E-6	(1.97± 0.02)E-6	(2.93± 0.13)E-1	(6.07± 1.18)E-1	(3.93± 0.11)E-2	(4.33± 0.06)E-2	(-.2.14± 1.12)E-2	(-3.22± 1.31)E-1
27	50:1dPPP(90)/KZ23	0.01449	10	0.625	58	105.39	(1.05± 0.03)E-5	(8.11± 0.02)E-7	(7.05± 0.02)E-7	(7.07± 0.01)E-7	(3.30± 0.10)E0	(2.55± 0.01)E-1	(2.22± 0.01)E-1	(2.22± 0.00)E-1	(-3.32± 0.12)E-2	(-1.27± 0.04)E-1
28	50:1dPPP(90)/NH4Z23	0.01675	10	0.625	51.46	111.67	(1.32± 0.00)E-6	(2.63± 0.04)E-7	(1.62± 0.04)E-7	(2.08± 0.10)E-7	(3.58± 0.01)E-1	(7.14± 0.11)E-3	(4.41± 0.10)E-3	(5.66± 0.03)E-2	(-2.73± 0.17)E-3	(-3.68± 0.19)E-1
29	50:1dPPP(90)/HZ23	0.01353	10	0.625	52	150	(5.07± 0.38)E-6	(9.87± 0.02)E-7	(5.83± 0.02)E-7	(5.77± 0.01)E-7	(1.71± 0.01)E0	(3.33± 0.01)E-1	(1.96± 0.01)E-1	(1.94± 0.00)E-1	(-1.36± 0.01)E-1	(-4.08± 0.03)E-1
30	50:1dPPP(90)/HZ23	0.02023	10	0.625	85.42	38.77	(1.30± 0.06)E-5	(7.64± 0.38)E-7	(5.15± 0.05)E-1	(4.80± 0.07)E-7	(2.92± 0.13)E0	(1.72± 0.09)E-1	(1.16± 0.01)E-1	(1.08± 0.02)E-1	(-5.61± 1.00)E-2	(-3.20± 0.61)E-1

Appendix L Ammonia Temperature Programmed Desorption

An ammonia temperature programmed desorption (NH_3-TPD) of zeolite was performed in a flow-through reactor with helium as a carrier. In order to remove water and undesired impurities, approximated 0.05 g of sample was pre-treated under He flow by heating from 30 °C to 500 °C at 10 °C/min. After holding temperature at 500 °C for 1 h and cooling to ambient temperature, the gas flow was switched to 1% NH_3/He. The NH_3 adsorption under room temperature was allowed for 1 h and the removal of weakly adsorbed NH_3 was then achieved by purging He gas into the system for 2 h. The NH_3 desorption was done by elevating temperature from 30 °C to 600 °C at ramp rate of 10 °C/min. In case of dPPP, NH_3 desorption was performed by elevating temperature from 30 °C to 300 °C. The desorbed NH_3 was detected by thermal conductivity detector (TCD).

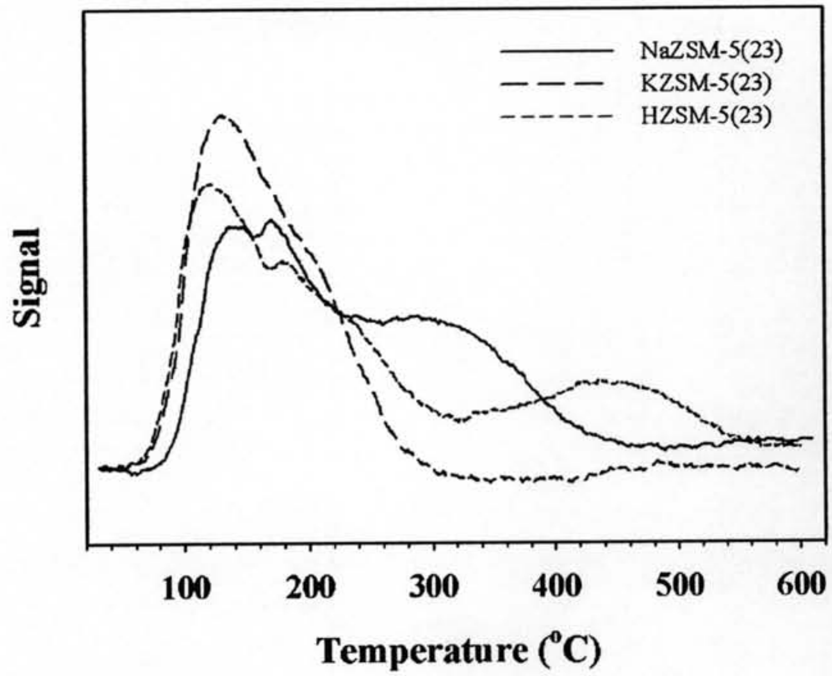

Figure L1 NH_3-TPD thermogram of ZSM-5(23) with various cation types.

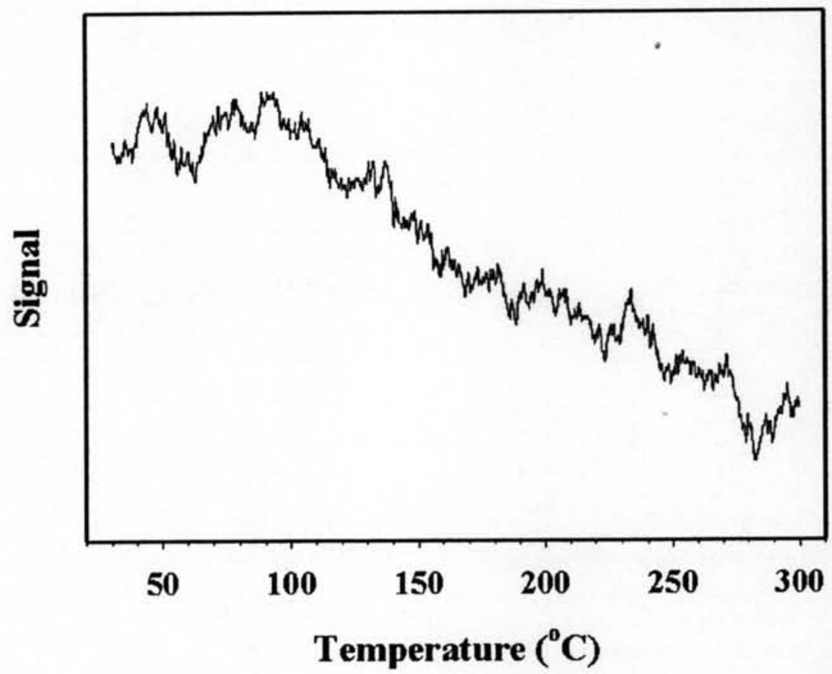

Figure L2 NH_3-TPD thermogram of 50:1 dPPP.

Appendix M Investigation of Interaction between dPPP, dPPP composite, NaZSM-5(23) and NH_3 by using FTIR technique

FTIR spectra of 50:1 dPPP, 50:1dPPP(70)/NaZ23 and NaZSM-5(23) were taken by using KBr pellet technique. The sample pellet was located on sample holder and put in the gas cell. The spectra of samples were collected, before, during and after NH_3 exposure, in order to study the interaction between these samples and NH_3.

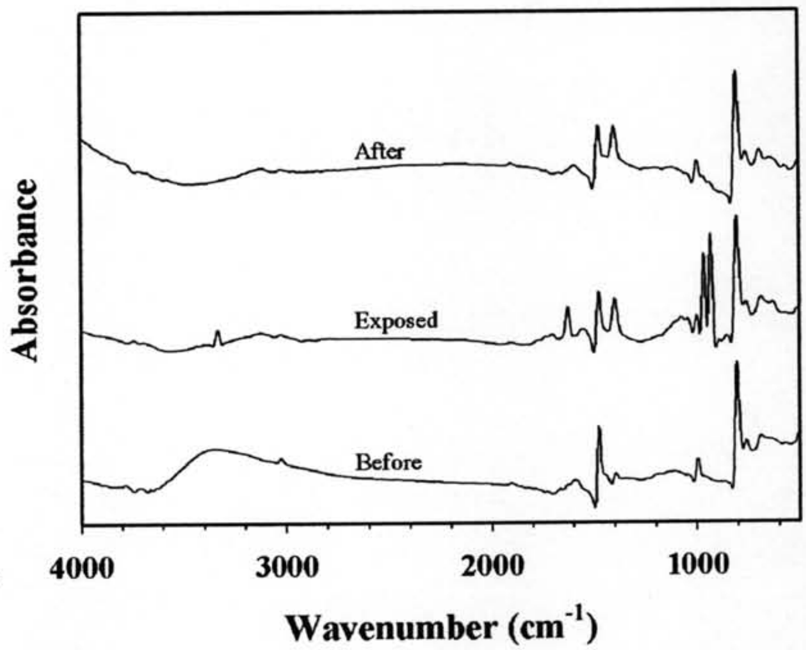

Figure M1 The FT-IR spectra of 50:1dPPP; before, during and after NH_3 exposure.

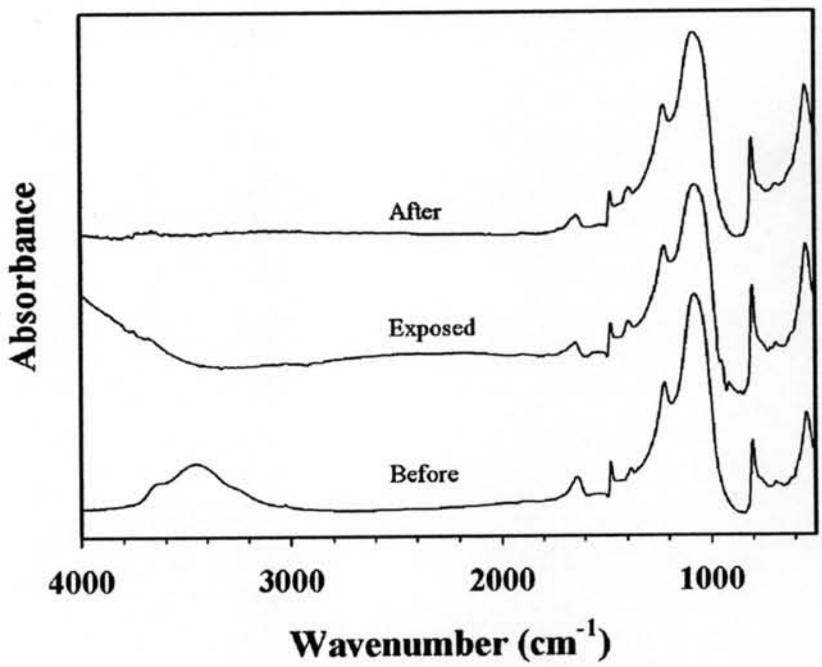

Figure M2 The FT-IR spectra of 50:1dPPP(70)/NaZ23; before, during and after NH_3 exposure.

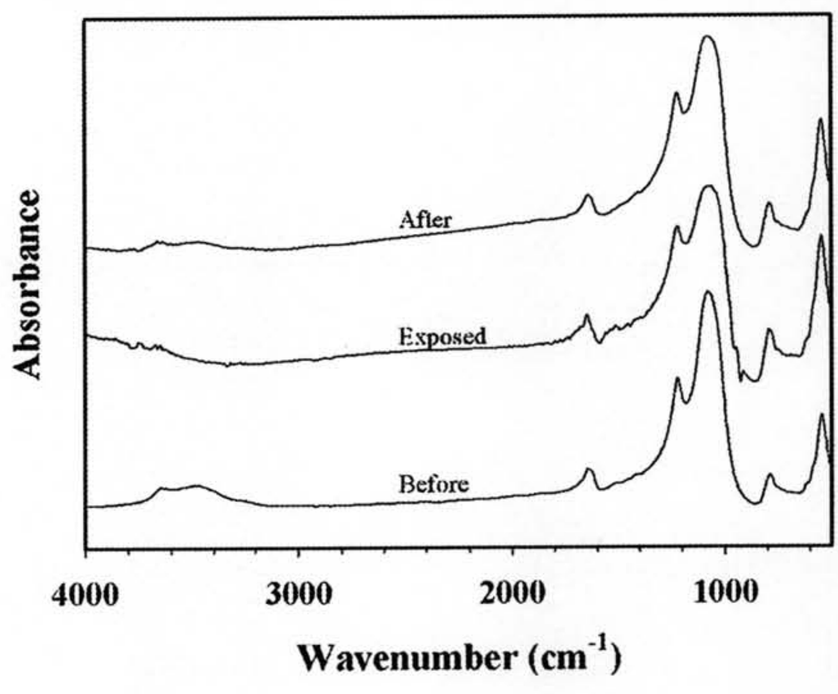

Figure M3 The FT-IR spectra of NaZSM-5(23); before, during and after NH_3 exposure.

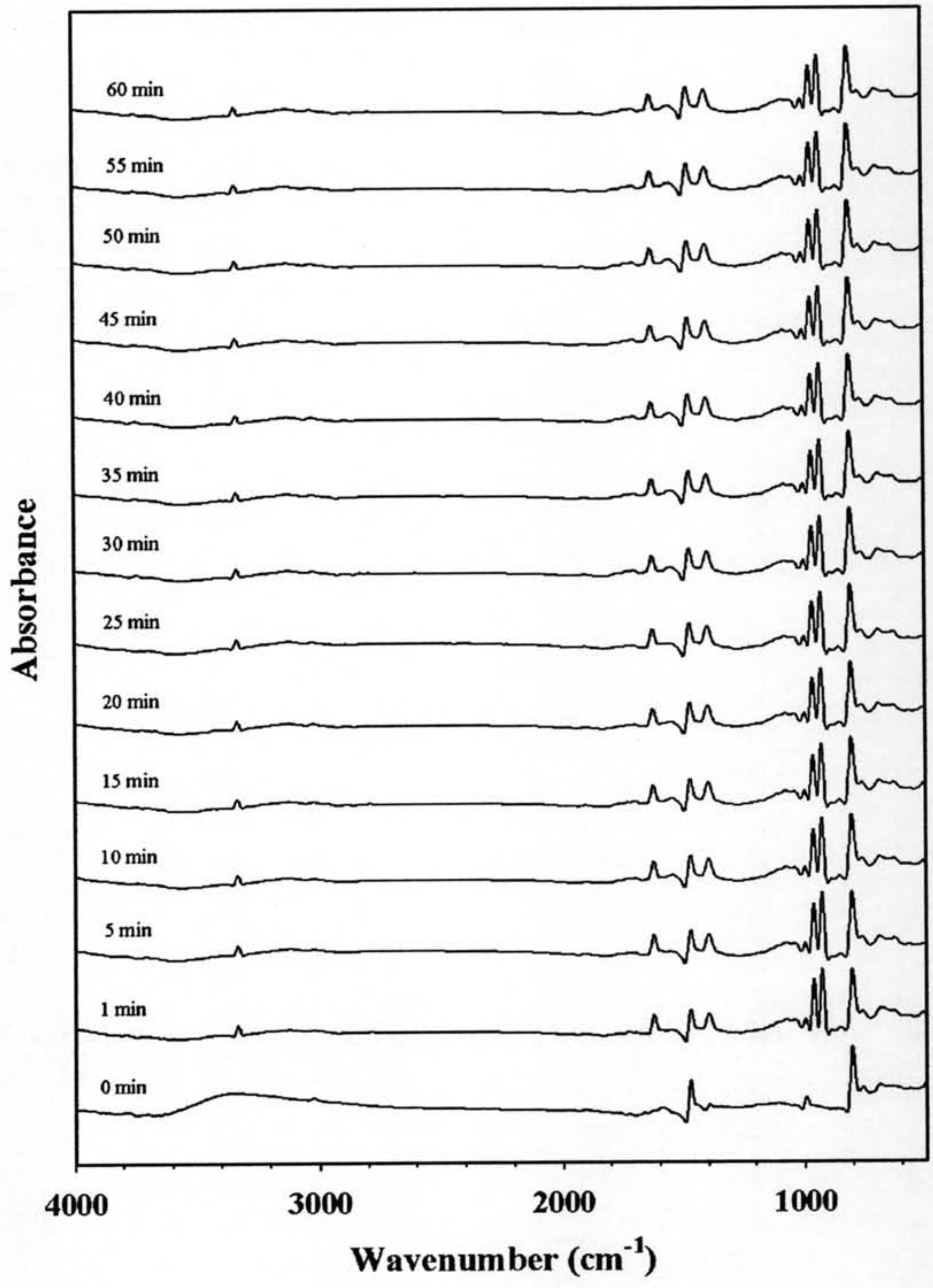

Figure M4 The FT-IR spectra of 50:1dPPP versus time of NH_3 exposure.

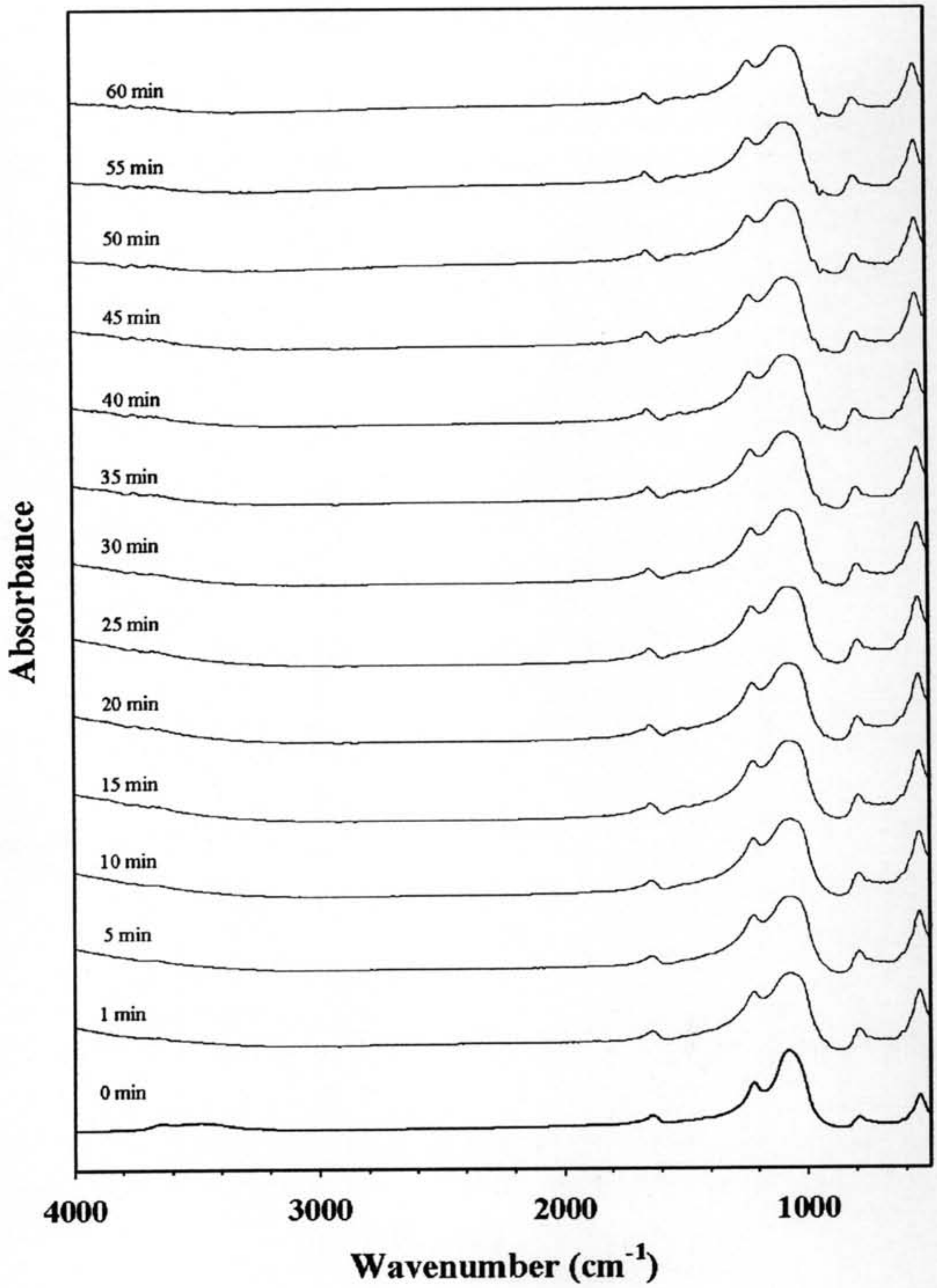

***Figure* M5** The FT-IR spectra of NaZSM-5(23) versus time of NH_3 exposure.

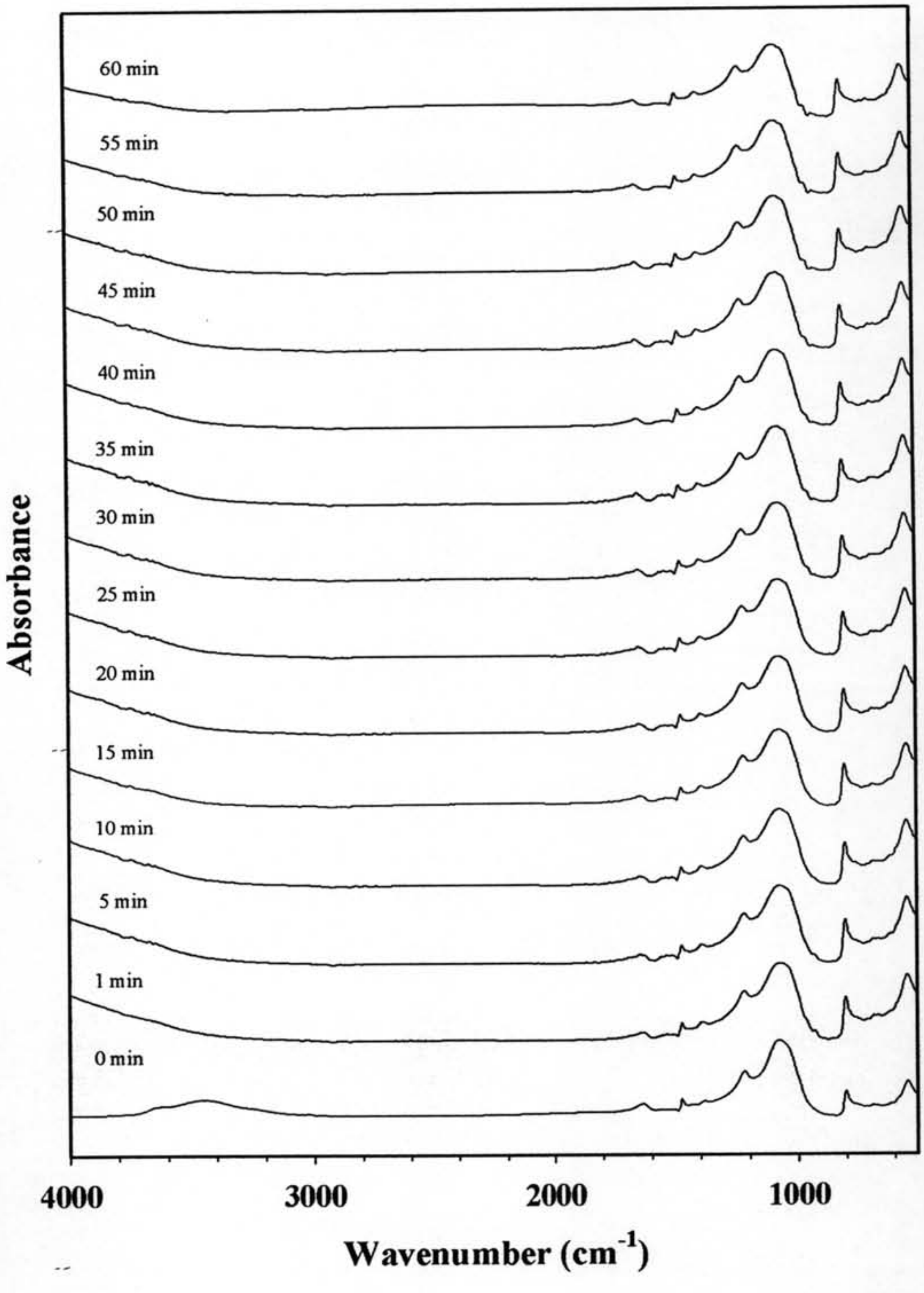

Figure M6 The FT-IR spectra of 50:1dPPP(70)/NaZ23 versus time of NH_3 exposure.

Table M1 Peak position in FT-IR spectra of 50:1dPPP before, during and after NH_3 exposure

Characteristic bands	Ref. (cm^{-1})	Wavenumber (cm^{-1})		
		before	exposed	after
NH_3 vibration	3336[a,b]	-	3333.06	-
C-H stretching of aromatic	3029[c]	3021.6	3021.6	3021.6
NH_3 vibration	1627.5[a,b]	-	1624.47	-
Quinoid structure	1600[d]	1593	1554	1592
C-C stretching of aromatic	1480[d]	1475.8	1474.25	1473.96
NH_3 vibration	1397[b]	-	1398.5	1399.3
C-H in-plane vibration of para disubstituted phenyl rings	1000[e]	995.9	998.7	995
NH_3 vibration	968.1[a,b]	-	964.3	-
NH_3 vibration	931.6[b]	-	929.5	-
C-H out of plane vibration of para disubstituted phenyl rings	817-805[f]	803.7	803.5	803.2
C-H out of plane vibration mono substituted phenyl rings	760[g]	760.7	757.8	760.0
C-H out of plane vibration of mono substituted phenyl rings	692[h]	688.5	687.7	691.5

Table M-2 Peak position in FT-IR spectra of NaZSM-5(23) before, during and after NH_3 exposure

Characteristic bands	Ref. (cm^{-1})	Wavenumber (cm^{-1})		
		before	exposed	after
Silanol group	3638[i]	3645	-	3662
	N/A	1642	1645.6	1640.5
Vibrations of T-O-T linkages	1232[i]	1222	1222.8	1223.3
Vibrations of T-O-T linkages	1062[i]	1079	1063.2	1077.8
NH_3 vibration	968.1[a,b]	-	951.8	-
NH_3 vibration	931.6[b]	-	916.4	-
Vibrations of T-O-T linkages	797[i]	790	792.6	791
Vibrations of T-O-T linkages	581[i]	544	544.6	544

Table M3 Peak position in FT-IR spectra of 50:1dPPP(70)/NaZ23 before, during and after NH_3 exposure

Characteristic bands	Ref. (cm^{-1})	Wavenumber (cm^{-1})		
		before	exposed	after
Silanol group	3638[i]	3639	-	3663
	N/A	1638	1645.1	1640.2
C-C stretching of aromatic	1480[d]	1479	1475.7	1476
NH_3 vibration	1397[b]	1383	1392.2	1387.2
Vibrations of T-O-T linkages	1232[i]	1223	1223	1223
Vibrations of T-O-T linkages	1062[i]	1078	1079.7	1078
NH_3 vibration	968.1[a,b]	-	950.9	-
NH_3 vibration	931.6[b]	-	916.4	-
C-H out of plane vibration of para disubstituted phenyl rings	817-805[f]	803	803.3	803.4
C-H out of plane vibration of mono substituted phenyl rings	692[h]	692	690.2	688.1
Vibrations of T-O-T linkages	581[i]	543	545.1	543.9

[a]Su, *et al.,* 2000, [b]Yin *et al.,* 1997, [c]Dale, 1957 and Castiglioni *et al.*, 1989, [d]Pham et al., 1990, [e]Soubiran *et al.*, 1998, [f]Froyer *et al.*, 1985, [g]Kvarnstrom *et al.* 1985, [h]Rakovic *et al.*, 1991, [i]Venkatathri N., 2006

CURRICULUM VITAE

Name: Ms. Pimchanok Phumman

Date of Birth: August 6th, 1982

Nationality: Thai

University Education:

2001-2005 Bachelor Degree of Science, Faculty of Science, King Mongkut's Institute of Technology of Ladkrabang. Bangkok, Thailand